Bio-Design and Manufacturing (2026) 9:357–378
https://doi.org/10.1631/bdm.2500348

RESEARCH ARTICLE

An integrated cartilage-on-a-chip recapitulating the bio-chemo-mechanical microenvironment in osteoarthritic joints

Hongxing Jia[1] · Shaohua Yang[1] · Lamei Du[1] · Han Gao[1] · Kaiqiang Sun[1] · Fanrui Kong[1] · Tan Tang[1] · Qiuting Zhang[1] · Tujun Weng[2] · Ye Xu[1]

Received: 10 July 2025 / Accepted: 14 November 2025

Abstract

Osteoarthritis (OA), the most common chronic joint disease, leads to remarkable morbidity and disability. The development of preclinical models that accurately recapitulate the bio-chemo-mechanical microenvironment of osteoarthritic joints is crucial for elucidating OA pathogenesis and facilitating drug development. In this study, we present a microfluidics-based cartilage-on-a-chip model that integrates tunable mechanical stimulation and inter-tissue/cell communication, mimicking the key physiological characteristics of articular cartilage for organ-level OA research. By applying controllable mechanical compression, we established a model that captures healthy and injury hallmarks of the cartilage and directly observed the mechanotransduction responses in chondrocytes. We further demonstrated that mechanically damaged cartilage induces synovial abnormalities and immune dysregulation and explored the potential of our chip as a platform for screening therapeutic targets. This cartilage-on-a-chip offers an in vitro system with a close-to-in vivo microenvironment for investigating complex bio-chemo-mechanical interactions, paving the way for advanced studies on OA pathogenesis and drug screening.

Graphical abstract

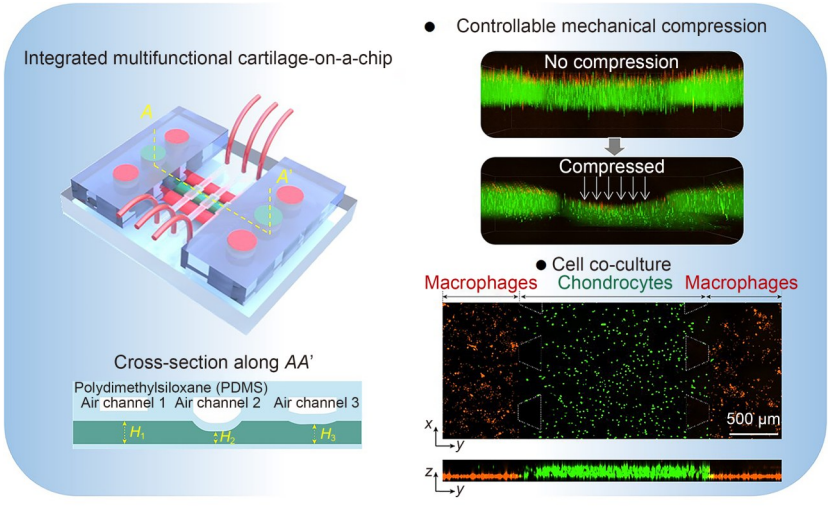

Keywords Osteoarthritis (OA) · Bio-chemo-mechanical coupled microenvironment · Cartilage-on-a-chip · Mechanical stimulation · Intercellular communications

✉ Tujun Weng
wengtujun@163.com

✉ Ye Xu
ye.xu@buaa.edu.cn

1 School of Mechanical Engineering and Automation, Beihang University, Beijing 102206, China

2 Senior Department of Orthopaedics, The Fourth Medical Center, Chinese PLA General Hospital, Beijing 100143, China

1 Introduction

Osteoarthritis (OA) is the most common chronic joint disease and is caused by various pathogenic factors, which include age, obesity, metabolic dysregulation, and genetic predisposition [1–7]. Despite its high prevalence, OA remains incurable, causing pain during daily activities, loss of joint function, and even disability. One of the major challenges in developing new therapies for OA is the complex joint microenvironment, where mechanical, biochemical, and cellular factors synergistically interact to initiate and exacerbate OA [1, 8–10]. For example, articular cartilage, a key tissue vulnerable to being affected by OA, is constantly subjected to mechanical loading from joint movements and is also influenced by biochemical factors such as immune cells and cellular secretions such as cytokines and chemokines [1]. Abnormal cartilage can disrupt the function of other tissues and cells within the joint microenvironment, further exacerbating OA development. This intricate interplay within the bio-chemo-mechanical joint microenvironment complicates the understanding of OA pathogenesis, making it challenging to develop effective disease models for pathogenesis elucidation and drug screening.

The current disease models for OA pathogenesis and drug screening are mainly built upon existing in vivo and in vitro methods. In vivo animal models can closely replicate naturally occurring whole-joint pathology and reflect the multifaceted nature of joint diseases. However, they are insufficient to indicate specific factors from the bio-chemo-mechanical-coupled microenvironment of the joints due to the limitations of existing in vivo research methods [1, 6, 11, 12]. Additionally, there are other drawbacks, such as high costs, long study durations, and ethical concerns that conflict with the 3R (reduction, refinement, and replacement) principles of animal model research. In vitro models, in contrast, offer advantages such as lower costs, simplicity, robustness, and high experimental reproducibility. In vitro models also enable detailed investigations of cellular processes under controlled conditions, allowing researchers to isolate specific factors from the bio-chemo-mechanical coupling within the joint microenvironment. Despite these advantages, current in vitro models do not adequately capture the dynamic interactions between the mechanical forces, biochemical signals, and cellular responses present in the joint microenvironment, which are critical to understanding OA. Therefore, there is a critical need for formulating new approaches that can mimic the in vivo physiological microenvironment more precisely, allowing for more accurate disease modeling and drug screening.

Organ-on-a-chip technology represents a promising approach to overcoming these challenges by reconstructing functional units that precisely mimic in vivo physiological microarchitecture and microenvironments within artificial microfluidic chips [11, 13–18]. Several types of microfluidic chips have been developed to model various organs, including the lung, liver, and heart, notably advancing disease modeling and drug screening applications [19, 20]. Recently, microfluidic chip models have been explored for investigating joint diseases, including OA [8, 21–29]. These chips are designed to apply mechanical stimulation, such as compression, to deform three-dimensional (3D)-cultured chondrocytes in hydrogel, for studying the effects of mechanical stimulation in OA [8, 22, 30, 31]. For example, Mainardi et al. [31] optimized mechanical stimulation to replicate tissue-specific loading (e.g., at the osteochondral interface) to study mechanical overload-induced OA traits. In addition, multicellular interactions during OA development (e.g., immunological processes such as cell migration and inter-tissue signaling) can be studied through multi-microchannel designs with integrated vascular or immune components [1, 24]. Based on these microfluidic designs, personalized platforms have been developed using patient-matched cells and synovial fluid for biological therapy screening [29]. While these microfluidic chips demonstrate the feasibility of investigating the processes involved in the onset and development of joint diseases, they have not been able to fully mimic the biochemical–mechanical joint microenvironment coupling and model the process that integrates mechanical cues with inter-tissue communication, which are critical to the onset and development of OA. Moreover, current models lack the key potential for real-time monitoring of cellular responses and inter-tissue communication under simultaneous mechanical overloading, which are crucial in understanding how mechanical cues drive OA onset and progression.

In this study, we developed an integrated cartilage-on-a-chip capable of recapitulating the physiological characteristics and bio-chemo-mechanical microenvironment of cartilage. Specifically, the biochemical microenvironment was replicated via spatially defined co-culture models to mimic intercellular crosstalk and endogenous bioactive molecule secretion. Meanwhile, the mechanical microenvironment was established through a precisely controlled loading module that delivers various levels of mechanical compression (e.g., the overload used for OA induction). By integrating these microenvironment recapitulations with in situ real-time visualization at the single-cell level, our chip forms a multifunctional microphysiological system for OA research. Using the cartilage-on-a-chip, we established a cartilage injury model to induce OA features via hyperphysiological mechanical stimulation. In addition, we observed the mechanotransduction responses, including mechanosensitive Piezo1 channel activation, calcium influx, and cytoskeleton reorganization. We also established two co-culture models, namely, a cartilage–synovium co-culture model and a cartilage–macrophage co-culture model, to simulate the inter-tissue/cell communication during the process of OA onset and development. In addition, we validated the multifunctional chip as a tool for

screening potential therapeutic targets in mechanically overloaded chondrocytes. The results demonstrated the potential of the cartilage-on-a-chip for studying the pathological processes involved in the onset and development of OA and evaluating potential therapeutic targets and drug candidates.

2 Results and discussion

2.1 Establishment of the microenvironment of articular cartilage with integrated mechanical and biochemical stimulation in a chip

To recapitulate the intricate bio-chemo-mechanical coupled microenvironment that chondrocytes encounter in vivo and investigate cellular behaviors across diverse temporal scales (Fig. 1a), we designed and fabricated an integrated multifunctional cartilage-on-a-chip based on a microfluidic device (Figs. 1b and 1c). As shown in Fig. 1d and Fig. S1 (supplementary information), the device consists of four layers: the ultra-thin glass substrate layer, the cell culture layer, the layer with air-loading compartments, and the top layer containing three reservoirs connecting to the cell culture channels. The key structural features used to realize mechanical loading and co-culture capabilities are illustrated in Figs. 1e and 1f. The cell culture layer comprises three channels separated by trapezoidal micropillars, where the middle channel is used for 3D cell culture, whereas the two side channels serve for medium supply or additional cell culture. These discontinuously arranged trapezoidal micropillars act as effective boundaries to confine the hydrogel within the middle channel, while still permitting substance exchange between the channels. A pressurization actuation compartment is tightly affixed above the cell culture layer. This compartment is designed to generate mechanical compression on the underlying 3D cell culture. Mechanical compression is achieved by pressurizing the air within the chambers, which induces deformation of the thin polydimethylsiloxane (PDMS) membrane positioned between the air chamber and the 3D cell culture channel (Fig. 1e). Notably, the air-loading channels and underlying cell culture channels are arranged orthogonally (Figs. 1d and 1e), enabling control over the regions where mechanical compression is applied to the 3D cell culture directly beneath the overlapping rectangular areas of the air channels.

To establish an articular cartilage model, we used an ultraviolet (UV)-curable gelatin methacryloyl (GelMA) hydrogel to mimic the extracellular matrix (ECM). Specifically, we injected a mixed solution of chondrocytes and hydrogel into the middle channel of the cell culture layer and then cured it using UV light, forming a 3D cartilage-like microconstruct. The chondrocytes were found to be uniformly distributed within the hydrogel (Fig. 1g). Importantly, the chondrocytes within the hydrogel exhibited a spherical morphology, with filamentous actin (F-actin) predominantly concentrated at the periphery of the cell membrane. In contrast, the chondrocytes in a conventional two-dimensional (2D) cell culture dish demonstrated longer and broader F-actin and a larger cell spreading area (Fig. 1h). These results indicate that the GelMA hydrogel resembled the chondrocyte ECM in our chip.

To validate the chip's mechanical compression capability, we visualized hydrogel deformation via green fluorescent nanoparticles incorporated into the hydrogel. Meanwhile, red fluorescent nanoparticles were attached to the PDMS membrane surface to visualize its deformation. Upon the introduction of compressed air into the air channel, we observed deformation of the PDMS membrane and vertical compression of the underlying hydrogel (Fig. 1i). As expected, compressed regions of the hydrogel in the middle channel of the cell culture layer were localized beneath the air channel as a result of the orthogonal design of the air-loading and cell culture channels.

In addition to the mechanical compression, our chip features a multichannel design to offer cell co-culture capability for the study of inter-tissue/cell communication. As a demonstration, we seeded macrophages into both side channels after establishing the 3D cartilage-like microconstruct in the middle channel, to mimic the in vivo spatial communication between chondrocytes in cartilage and macrophages in joint fluid. We labeled the chondrocytes with the green fluorescent dye, carboxyfluorescein succinimidyl ester (CFSE), and labeled the macrophages with the red fluorescent dye, 1,1'-dioctadecyl-3,3,3',3'-tetramethylindocarbocyanine perchlorate (DiI). We observed that macrophages (red) were attached to the bottom of the channels on both sides, whereas chondrocytes (green) were embedded in the hydrogel of the middle channel, with a clear spatial distribution boundary between the two types of cells (Fig. 1j). This visualization configuration of the two cell types within the chip emphasized the capability of the chip to mimic spatially compartmentalized cell distribution.

2.2 Precise control of mechanical compression onto 3D-cultured cells

One of the key functionalities of the multifunctional chip is the precise control of mechanical compression on 3D-cultured chondrocytes within the hydrogel. The compressed region within the chip can be accurately controlled due to the custom-designed multiple parallel air channels in the actuation compartment (Fig. 2a). We observed the deformation region of the hydrogel within the chip when two adjacent air channels were operated simultaneously. As an example, when an air pressure of 1000 mbar (1 mbar=100 Pa) was applied simultaneously to two adjacent air channels, deformation of the hydrogel occurred only in the region where the hydrogel

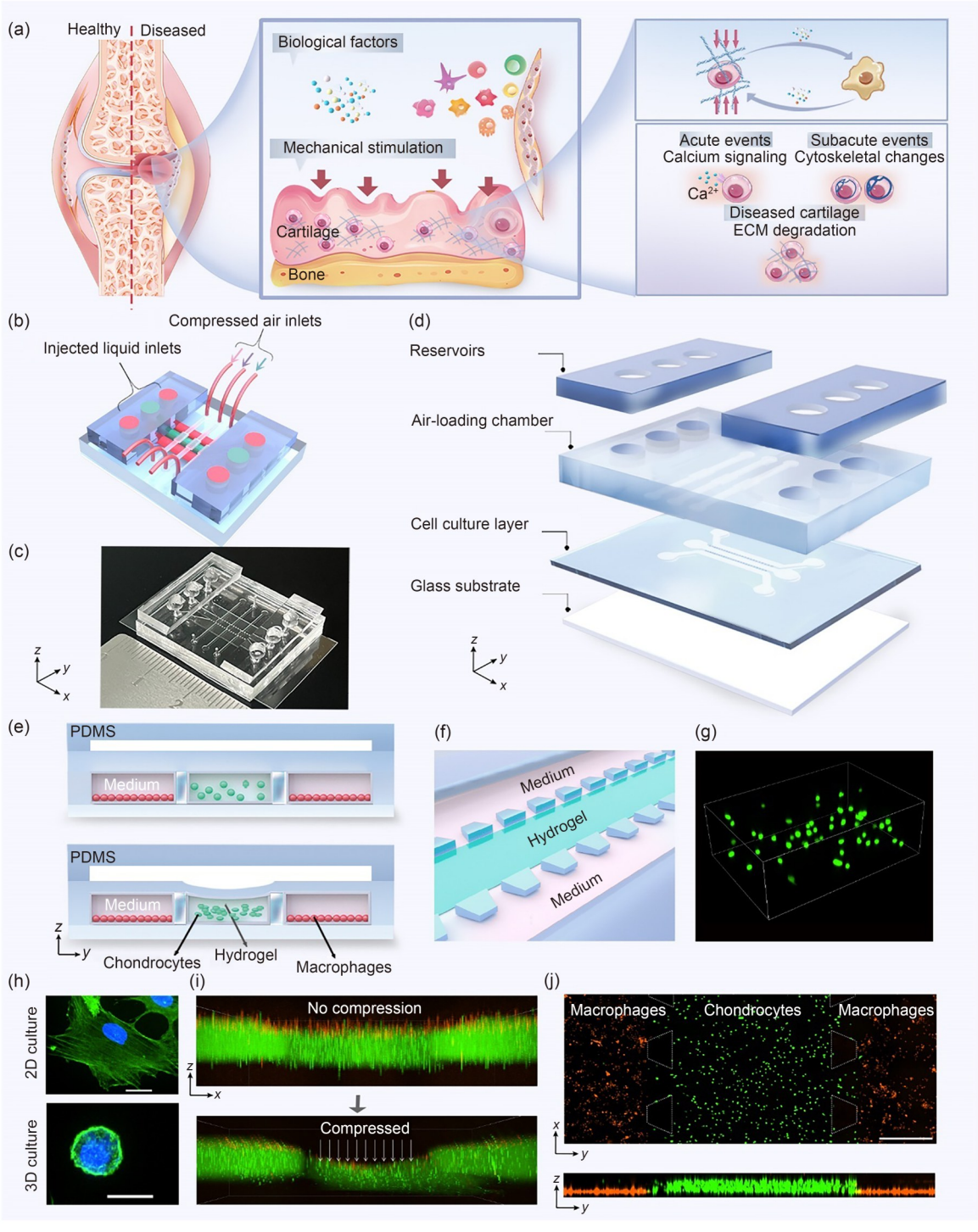

Fig. 1 Design and functional demonstration of an integrated cartilage-on-a-chip for simulating the microenvironment of articular cartilage with integrated mechanical stimuli and multicellular co-culture. (a) Schematic diagram of the bio-chemo-mechanical-coupled microenvironment and the complex cellular behavior within a diseased joint. (b) Schematic illustrating the design of the integrated cartilage-on-a-chip. (c) Representative photograph of the cartilage-on-a-chip. (d) Exploded-view drawing of the chip, comprising multiple layers. (e) Schematic 3D view depicting the configuration of mechanical compression and multicellular co-culture in the chip. (f) Enlarged schematic representation of the cell culture layer, featuring three channels separated by two rows of trapezoidal pillars. (g) 3D configuration of confocal Z-stack images depicting the spatial distribution of chondrocytes cultured within the hydrogel in the chip. (h) Representative confocal Z-stack maximum-intensity projection of immunofluorescence staining of the cytoskeleton in 3D-cultured chondrocytes (hydrogel, bottom) and 2D-cultured chondrocytes (culture dishes, top). Scale bars: 20 μm. (i) Confocal images demonstrating the deformation of the hydrogel (green) in the chip with mechanical compression. (j) Representative confocal maximum-intensity projection showing a co-culture of 3D-cultured chondrocytes (green) and 2D-cultured macrophages (red) in the chip. Scale bar: 500 μm

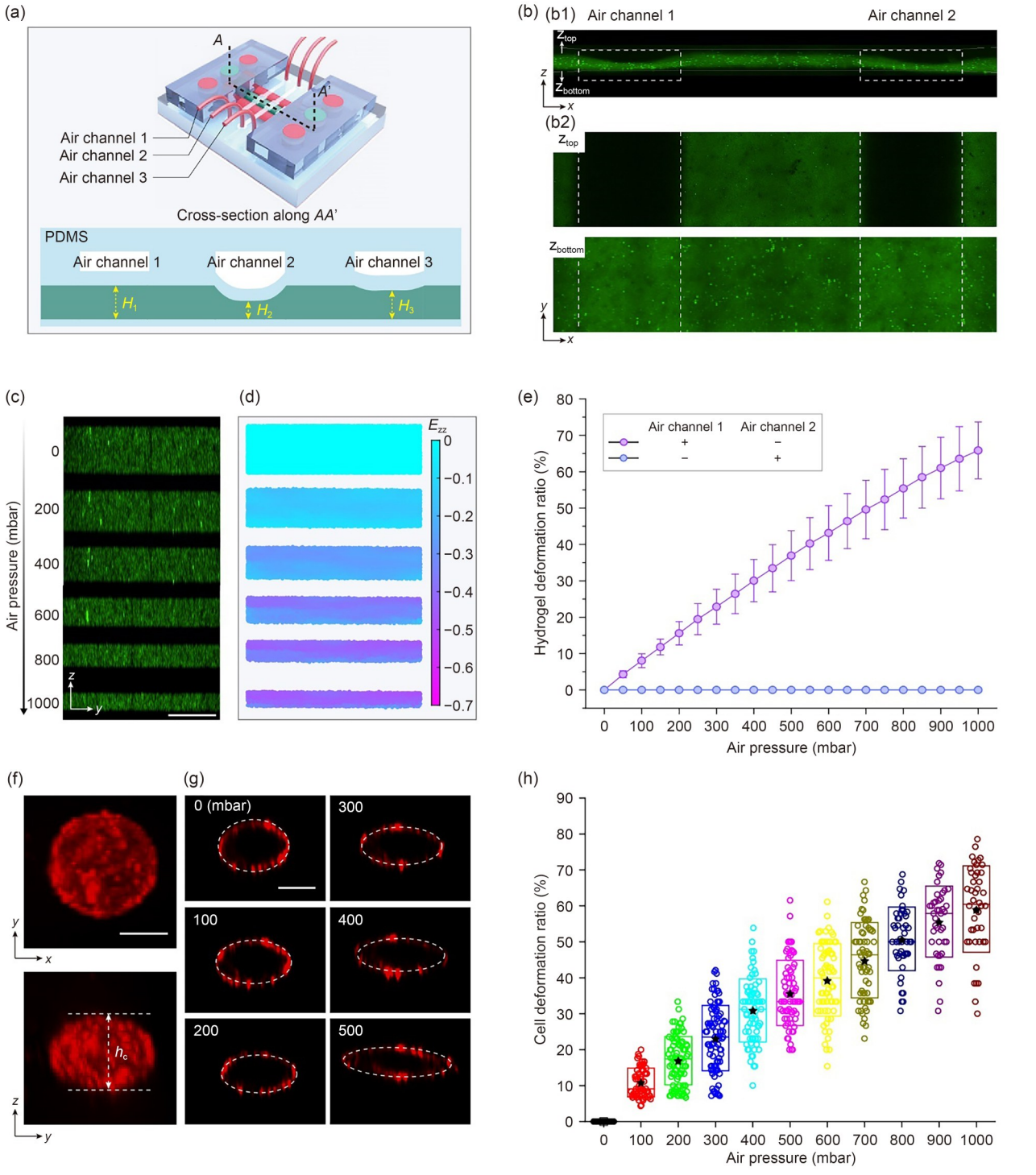

Fig. 2 Characterization of the mechanical compression function of the integrated cartilage-on-a-chip. (a) Schematic depiction illustrating the layout of multiple air channels enabling different customizable mechanical compression levels within the same chip. (b) Representative images showing the cross-sectional view (b1) and top–down view (b2) of the hydrogel within the chip upon the application of 1000 mbar of pneumatic pressure to two adjacent air channels (n=3 independent experiments). (c) Representative cross-sectional images showing the hydrogel deformation under varying air pressures. Scale bar: 100 μm. (d) The corresponding E_{zz} fields in the compressed hydrogel under varying air pressures. (e) The deformation ratio of the hydrogels underneath air channel 1 as a function of the applied air pressure introduced only in air channel 1 (purple line) and that introduced only in air channel 2 (blue line) (n=6). Data are presented as mean±standard error of the mean (SEM). (f) 3D view (top and side) of a 3D-cultured chondrocyte labeled with the fluorescent dye 1,1'-dioctadecyl-3,3,3',3'-tetramethylindodicarbocyanine,4-chlorobenzenesulfonate salt (DiD) in the chip. Scale bar: 10 μm. (g) Representative images illustrating the deformation of a single chondrocyte under different air pressures. Scale bar: 10 μm. (h) Quantification of chondrocyte deformation under different air pressure levels (n=85). ★: mean values; top and bottom lines of the box: SEM; middle line of the box: median value. 1 mbar=100 Pa

channel vertically overlapped with the air channel. This local deformation was characterized by a reduction in the hydrogel thickness (Fig. 2b1) and the out-of-focus nature of the fluorescence particles embedded within the top layer of the hydrogel in the confocal images (Fig. 2b2).

In addition to the custom-designed compressed region, the deformation of the hydrogel can be precisely controlled. As shown in the confocal 3D-reconstructed images in Fig. 2c, the thickness of the hydrogel gradually decreases with an increase in pressured air in the air channels positioned above. We further quantified the spatial distribution of the compressive strain by analyzing the 3D confocal images of the hydrogel under varying compression (Fig. S2 in the supplementary information) (see Sect. 4.4 for more details). As shown in Fig. 2d, the compressed strain (E_{zz}) of the hydrogel increases with the applied air pressure, and the distribution of E_{zz} was relatively uniform in the hydrogel within the observed region. We then defined the compressive deformation of the hydrogel (ε_g) as follows:

$$\varepsilon_g = \left(h_{g0} - h_g\right)/h_{g0}, \tag{1}$$

where h_g represents the thickness of the hydrogel after mechanical compression and h_{g0} represents the initial thickness of the hydrogel. The results indicated that the compressive deformation ratio increased with higher air pressure, as shown by the purple line in Fig. 2e. Also, when the compressed air pressure reached 400 mbar, the hydrogel's compressive deformation ratio reached approximately 30%, a cutoff between the physiological and hyperphysiological compression for articular cartilage, as previously defined in Ref. [8]. In addition, the independent control of localized mechanical loading was verified by comparing the compressive strain of hydrogels underneath two different air-loading channels. As shown in Fig. 2e, while the pressure applied to one air channel increased, which resulted in an increase in the compression ratio of the hydrogels directly underneath, the hydrogel under the adjacent channel, where no air pressure was applied, did not show any visible compression.

Next, we investigated the deformation of chondrocytes that were uniformly dispersed within the hydrogel under air pressure-driven compression. By labeling the cell membranes of the chondrocytes (Fig. 2f), we observed changes in chondrocyte morphology following compression. We defined the cell thickness (h_c) as the dimension of the cells along the direction of hydrogel compression and quantified the deformation by analyzing the cell surface outline (Fig. 2g). Cell deformation (ε_c) was defined as follows:

$$\varepsilon_c = (h_{c_0} - h_c)/h_{c_0}, \tag{2}$$

where h_c and h_{c_0} represent the measured cell thickness after and before compression, respectively. The results shown in Fig. 2h demonstrate increasing compression of 3D-cultured cells with increasing air pressure. Notably, ε_c exhibited good agreement with ε_g (Fig. S3 in the supplementary information), indicating that an effective mechanical loading was applied to cells embedded in the hydrogel. Together, these results demonstrate that our chip, with its custom-designed actuation compartment, can precisely control the level and location of mechanical compression to the hydrogel and 3D cells.

2.3 Establishment of mechanically-regulated differentiated models featuring healthy and osteoarthritic traits within a single chip

We established a model with the capacity to precisely control the magnitude and spatial distribution of mechanical compression so that it simultaneously captures the healthy and osteoarthritic hallmarks of cartilage within a single cartilage-on-a-chip to simulate the physiological and hyperphysiological mechanical loading to cartilage during joint movement (Fig. 3a). We designed an experimental protocol (Fig. 3a1) following established methodologies for chondrocyte anabolism and catabolism [8, 22]. This model focuses on monitoring chondrocyte metabolic responses to mechanical stimuli within a mechanically representative matrix. Specifically, we constructed a hydrogel-based 3D cartilage-like microconstruct in the chip and maintained static culture for 7 d. Subsequently, mechanical compression was applied to the hydrogel-embedded cells for 14 d. The chip's custom-designed mechanical loading feature allowed independent control of three air pressure channels, enabling the application of distinct air pressure levels to different regions of the hydrogel.

We applied 100 mbar of air pressure to the air channels on both sides to simulate physiological mechanical compression (PC) to model the health characteristics of cartilage, while applying 600 mbar to the middle air channel to induce hyperphysiological mechanical compression (HPC) to model the injury characteristics of cartilage (Fig. 3a2). To simulate the compression applied during a slow walk at low daily activity levels, dynamic air pressure with a sinusoidal waveform with a frequency of 0.5 Hz (Fig. 3a3) was employed for a 4-h loading period per day from Day 7 to Day 21. Throughout the duration of the experiment, chondrocytes demonstrated notable viability, as evidenced by live/dead staining of chondrocytes cultured for 7 and 21 d, respectively (Fig. 3b). To further quantify proliferation and track cell health over time, we counted cells using Hoechst-stained nuclei at 0, 7, and 21 d post-seeding. Cell numbers showed no significant differences across these time points (Fig. S4 in the supplementary information), indicating that the chondrocyte population remained stable over the 21-d culture period. This stability aligned with the known in vitro phenotype of chondrocytes with limited proliferation but sustained viability, supporting the stability of the engineered cartilage model in the chip under the tested compression conditions.

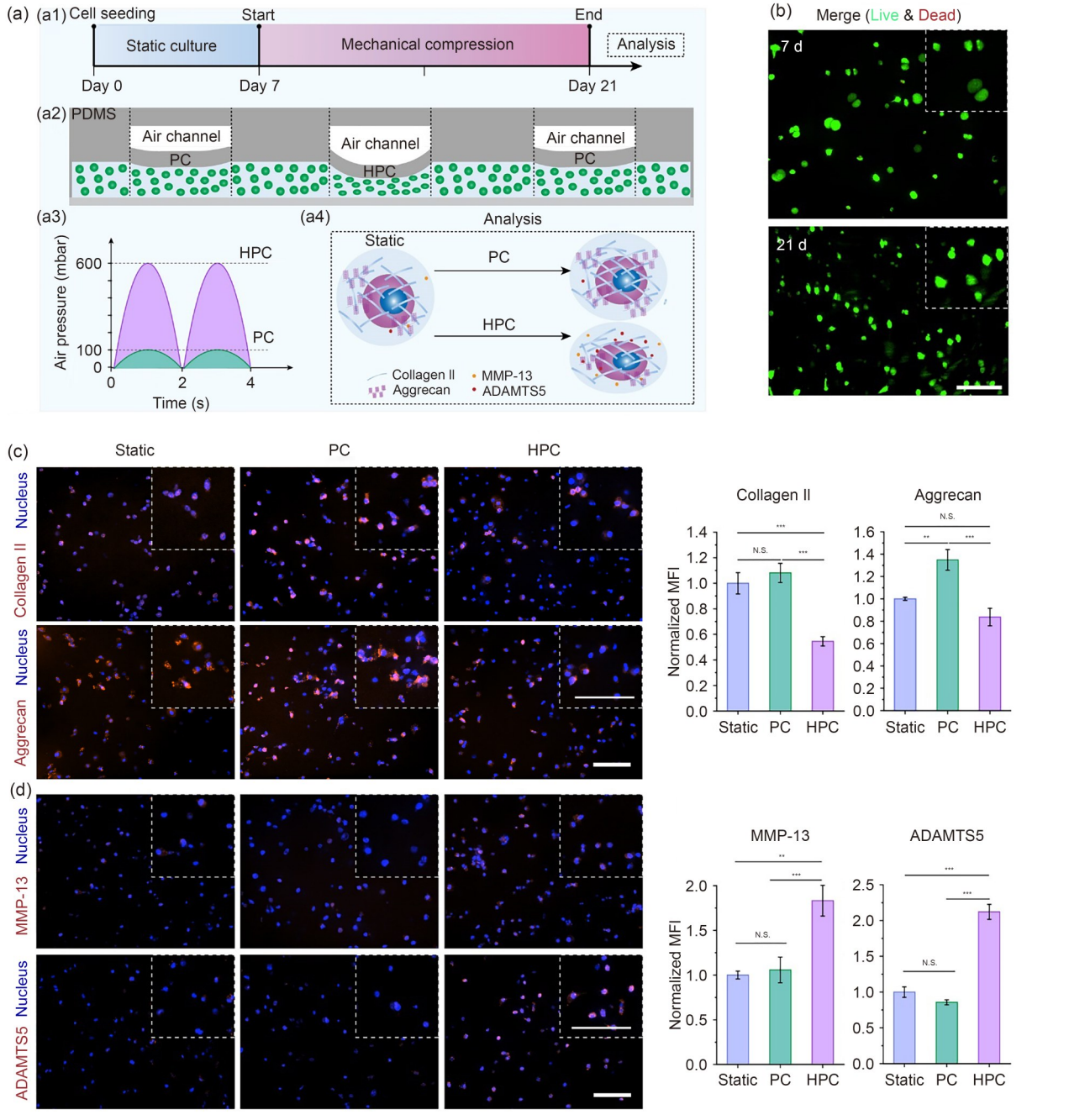

Fig. 3 Establishment of mechanically regulated cartilage health and injury models within a single cartilage-on-a-chip. (a) Schematic showing the experimental timeline (a1), the mechanical compression levels in three air channels in one chip (a2), the application cycles of mechanical stimulation (a3), and the evaluation of the model after mechanical stimulation (a4). (b) Representative confocal Z-stack maximum-intensity projection displaying the cell viability of chondrocytes cultured for 7 and 21 d in the hydrogel within the chip. Scale bar: 100 μm. (c) Representative confocal images and quantitative analysis of collagen II and aggrecan immunofluorescence in chondrocytes under different levels of mechanical compression within the microfluidic chip. Scale bars: 100 μm. (d) Representative confocal images and quantitative analysis of MMP-13 and ADAMTS5 immunofluorescence in chondrocytes under different levels of mechanical compression within the microfluidic chip. Scale bars: 100 μm. Data are presented as mean±standard error of the mean (n=3 independent experiments). Statistical significance was determined by one-way analysis of variance (ANOVA), followed by Tukey's post hoc test for pairwise comparisons. $^{**}p<0.01$ and $^{***}p<0.001$; N.S.: nonsignificant

After completing mechanical stimulation, we embedded the chondrocytes in the chip to assess their anabolic and catabolic activities, processes that are closely linked to chondrocyte dysfunction in OA. We employed immunofluorescence staining to assess the level of production of collagen II and aggrecan (Fig. 3a4), key markers of cartilage and crucial indicators of chondrocyte anabolism [8, 32]. In addition, we detected the expressions of matrix metalloproteinase-13

(MMP-13), and a disintegrin and metalloproteinase with thrombospondin motif 5 (ADAMTS5), which are the main matrix-degrading enzymes produced by chondrocytes under mechanical injury. These enzymes are linked to chondrocyte catabolism and contribute to the progressive cartilage degradation seen in OA [4, 8, 33].

The immunofluorescent staining results revealed a marked increase in the expression of collagen II and aggrecan for chondrocytes in the PC group (Fig. 3c). In contrast, a notable downregulation in expression for chondrocytes in the HPC group was observed. Statistical analysis of the normalized mean fluorescence intensity (MFI), derived from the immunofluorescence data, revealed significant between-group differences in collagen II and aggrecan expression levels. In addition, chondrocytes in the region subjected to HPC exhibited higher expression levels of MMP-13 and ADAMTS5 compared to the PC region on the same chip, whereas chondrocytes in the PC group showed no significant difference compared to the static group (Fig. 3d). These observations align with those of previous studies that demonstrated that physiological mechanical stimulation activates chondrocyte anabolic pathways, whereas mechanical overload promotes catabolic activity [8, 22].

Notably, 10% (0.1 g/mL) GelMA was used as the 3D culture matrix (Fig. S5 in the supplementary information). While GelMA is commonly used to mimic native cartilage, its dense network may inherently restrict ECM deposition. Given this characteristic, the upregulation of collagen II and aggrecan expressions in the PC group reflects an activated anabolic trend in chondrocytes rather than direct evidence of extensive ECM accumulation. That said, these trends in marker expression are sufficient to compare the chondrocyte metabolic responses to different mechanical stimuli, which in turn highlights the key functional validation of the chip. These region-specific differences in the expressions of anabolic (collagen II and aggrecan) and catabolic (MMP-13 and ADAMTS5) markers ultimately demonstrate functional anastomosis between controllable mechanical compression and mechanically regulated cartilage homeostasis.

It is also important to highlight that because of the unique design of the three air channels being placed orthogonally to the 3D cell culture channel (Fig. 2), we can independently control the magnitude, duration, frequency, and type of mechanical compression applied to the cartilage-like microconstruct only within the designated regions. This feature allows us to directly compare cellular responses under different mechanical compression conditions (i.e., static, PC, and HPC) within the same chip, therefore minimizing between-sample variations. Furthermore, this localized mechanical loading capability can be used to mimic non-uniform stress distribution on the articular cartilage, which is common in the case of subchondral bone structural alterations [32, 34]. Using the spatially localized cartilage models that feature healthy and osteoarthritic traits within a single chip, we can potentially compare chondrocyte responses in high-stress and low-stress regions, thus elucidating the site-specific onset of OA under specific pathological conditions such as obesity, trauma, and uneven joint stress [10, 35–37].

2.4 In situ visualization of 3D mechanotransduction responses in chondrocytes under mechanical overload

With the successful establishment of the osteoarthritic model with controllable mechanical compression, we further utilized the in situ microscopic observation capability of our chip to reveal the dynamic process of cellular responses under mechanical overloading. Specifically, we investigated several typical mechanotransduction responses (Fig. 4a) of 3D-cultured chondrocytes under mechanical overload, which plays a critical role in the initial stage of OA. We first evaluated the expression of Piezo1, a crucial mechanosensitive ion channel that mediates chondrocyte responses to injurious mechanical overload, on the cell membrane of chondrocytes subjected to such overload in the chip. The immunofluorescence results demonstrated that Piezo1 expression was 30% higher in compressed chondrocytes compared to uncompressed controls (Fig. 4b). This enhanced Piezo1 expression indicated that the 3D-cultured chondrocytes in our chip respond to mechanical overload and trigger mechanotransduction, consistent with the observations of previous studies that demonstrated that Piezo1 is implicated in the mechanotransduction of injurious mechanical stimuli [35, 38–40].

We also investigated the calcium influx (one of the earliest responses in mechanotransduction) into the chondrocytes during mechanical overload. To visualize calcium influx, we loaded the chondrocytes within the hydrogel along with a fluorescent probe Calbryte^{TM} 520 AM before applying mechanical compression. The intracellular calcium concentration was then quantified using the MFI of the chondrocytes. As shown in Fig. 4c, the intracellular calcium concentration inside the compressed region was markedly increased after HPC application for 270 min. Furthermore, the in situ microscopic observations allowed us to quantify the variation in the intracellular calcium concentration of each chondrocyte over time when subjected to mechanical compression. The time-lapse fluorescent micrographs of typical chondrocytes (Fig. 4d) demonstrated that the intracellular calcium concentration gradually increased under mechanical compression, reaching a peak at approximately 240 min and then decreasing sharply. This decline in intracellular calcium concentration after 240 min of mechanical overload was likely driven by intrinsic calcium homeostasis. Once cytosolic calcium reaches a physiological threshold, chondrocytes activate regulatory pathways, including plasma membrane pumps, that export excess calcium, as well as mechanisms

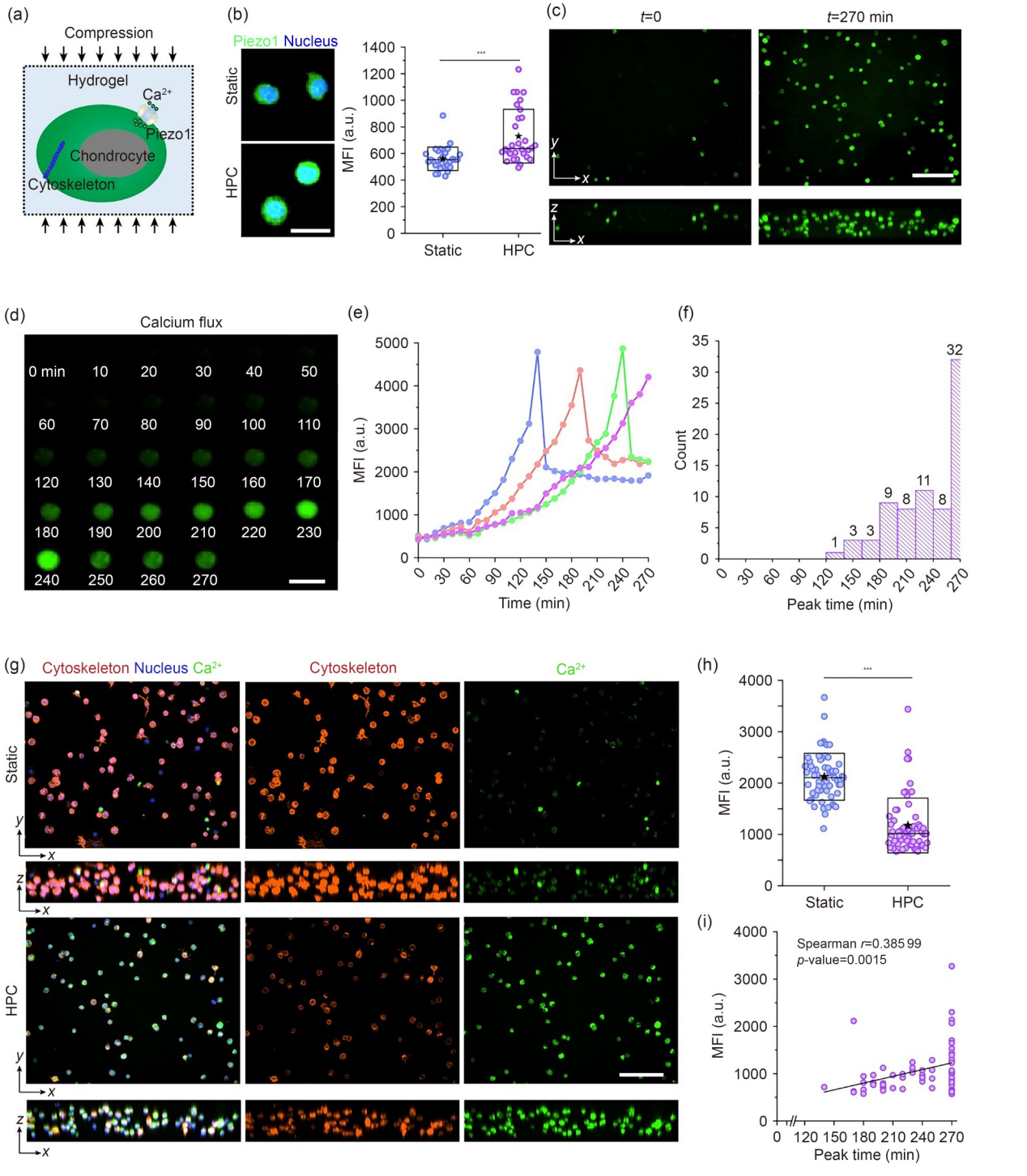

Fig. 4 In situ visualization of 3D mechanotransduction responses in chondrocytes under HPC in the chip. (a) Schematic showing the typical mechanotransduction responses of chondrocytes. (b) Representative confocal images and quantitative analysis of Piezo1 expression in 3D-cultured chondrocytes stimulated by HPC for 240 min (n=3 independent experiments). Scale bar: 20 μm. Statistical significance was determined by Student's t-test. $^{***}p<0.001$. (c) Representative confocal maximum-intensity projection showing the intracellular calcium ion concentration of 3D-cultured chondrocytes under HPC (left: 0 min; right: 270 min). Scale bar: 100 μm. (d) Confocal Z-stack maximum-intensity projection showing the intracellular calcium ion fluorescence intensity of single chondrocytes during HPC. Scale bar: 20 μm. (e) Temporal evolution of MFI of four representative chondrocytes under HPC. (f) Distribution of peak intracellular calcium ion concentrations at various time points during HPC. (g) Confocal maximum-intensity projection showing the cytoskeleton of 3D-cultured chondrocytes subjected to HPC for 270 min. Scale bar: 100 μm. (h) Quantification of the cytoskeleton in chondrocytes based on the fluorescence intensity in (g). Statistical significance was determined by Student's t-test. $^{***}p<0.001$. (i) Spearman's correlation analysis between the peak time of calcium influx and the cytoskeleton. ★: mean values; top and bottom lines of the box: standard deviation; middle line of the box: median value (for (b, h))

that sequester calcium into intracellular reserves (e.g., mitochondria) to restore the calcium levels to the baseline [3, 41].

The temporal evolution of intracellular calcium concentrations in four different chondrocytes is shown in Fig. 4e. Interestingly, although they shared the same trend in calcium concentration, each chondrocyte exhibited different peak times for calcium influx. The distribution of peak time for a total of 75 chondrocytes within the hydrogel under HPC is shown in Fig. 4f. The variation in the peak time of calcium influx among cells highlights the heterogeneity in the mechanotransduction of chondrocytes, owing to the presence of diverse chondrocyte subpopulations [42–45]. Taken together, the time-dependent changes in intracellular calcium concentrations, characterized by an initial increase and subsequent decrease, confirm that 3D-cultured chondrocytes embedded in the hydrogel can sense and respond to mechanical compression. This validates the cellular mechanical response of chondrocytes under mechanical overload and underscores the chip's capability for in situ visualization of 3D mechanotransduction processes at the single-cell level.

Because cytoskeleton force transmission is an essential mechanotransduction process in chondrocytes, we examined the cytoskeletons of chondrocytes subjected to HPC in our chip. Here, we used phalloidin staining to visualize the F-actin (a major cytoskeletal component) of chondrocytes within the hydrogel in the compressed regions. As shown in Figs. 4g and 4h, the F-actin fluorescence intensity of the chondrocytes in the compressed region was markedly lower than that in the uncompressed region, indicating possible cytoskeletal disruption caused by 270 min of HPC. This result was consistent with those of previous studies that demonstrated that mechanical overloading induces abnormal distribution and assembly (or even absence) of the cytoskeleton in chondrocytes [32, 35]. Meanwhile, the chondrocytes in the compressed region exhibited markedly higher intracellular calcium concentrations than those in the uncompressed region (Fig. 4g). This result suggests the relationship between intracellular calcium concentration enhancement and damaged F-actin induced by HPC in 3D-cultured chondrocytes. To confirm this, we used Spearman's correlation analysis to assess the relationship between the occurrence of calcium influx peaks and the cytoskeletal fluorescence intensity of chondrocytes and found a highly significant positive correlation ($r \approx 0.39$, $p = 0.0015$) (Fig. 4i). Our findings were consistent with those of previous studies that demonstrated that elevated calcium levels result in the rarefaction of the F-actin cytoskeleton [35, 40]. Therefore, our cartilage-on-a-chip model could be used as an experimental platform to further explore the complex mutual influence between calcium influx and F-actin, which would provide valuable insights into the mechanotransduction of chondrocytes under mechanical overload.

Taken together, these results demonstrate the capability of our cartilage-on-a-chip to serve as an integrated 3D biomimetic in vitro model for real-time monitoring of the earlier responses of chondrocyte mechanotransduction. Compared to existing microfluidic methods for studying mechanical responses in 3D chondrocytes, our chip offers the capability for in situ, real-time observation of the mechanically mediated calcium signaling and downstream responses [8, 28]. This integrated approach for investigating the mechanical response of cells is vital for advancing our understanding of the mechanotransduction of chondrocytes and for providing valuable insights into potential therapeutic targets [28, 35, 46].

2.5 Direct observation of multicellular interactions induced by mechanically overloaded cartilage injury

Our microfluidic chip platform enables real-time microscopic observation of chondrocyte mechanotransduction under mechanical compression and the establishment of a pathologically relevant co-culture model that recapitulates key stages of OA progression. This potential allows us to investigate inter-tissue/cell communication during mechanically induced OA initiation and development, such as between cartilage and synovium (key articular tissues) or macrophages (among the most abundant immune cells in the joints) [2, 47, 48].

As an example of functionality validation, we established a co-culture model of cartilage and synovium using the chip (Fig. 5a; Fig. S6 in the supplementary information). We examined the effects of mechanical overload-damaged chondrocytes on the synovium to demonstrate the pathological relevance of the co-culture model in OA progression. Specifically, upon subjecting chondrocytes to HPC (600 mbar, 0.5 Hz, 4 h per day) for 2 d, synovial fibroblasts, which constitute the major cellular components of the synovium, were injected into the side channels and seeded within the grooves among the PDMS trapezoidal pillars adjacent to the 3D cartilage-like microconstruct in the middle channel (see Sect. 4.3 for more details). For direct visualization via confocal microscopy, synovial fibroblasts were pre-labeled with the green fluorescent tracer, CFSE, prior to injection. This co-culture procedure established a direct contact interface between the cartilage and synovium (Fig. 5b; Fig. S7 in the supplementary information). Notably, the synovial fibroblasts within each groove of the PDMS trapezoidal pillars manifested an even distribution and a multilayered conformation, recapitulating the in vivo morphological characteristics of the synovium [1, 21].

We found that synovial fibroblasts co-cultured with mechanically overloaded chondrocytes exhibited invasive behavior. Specifically, on the same chip, synovial fibroblasts adhering to the compressed region of the cartilage-like microconstruct exhibited protrusions extending toward the chondrocyte culture at 17 h post-seeding, in contrast to those near the uncompressed region (Fig. 5c). These protrusions

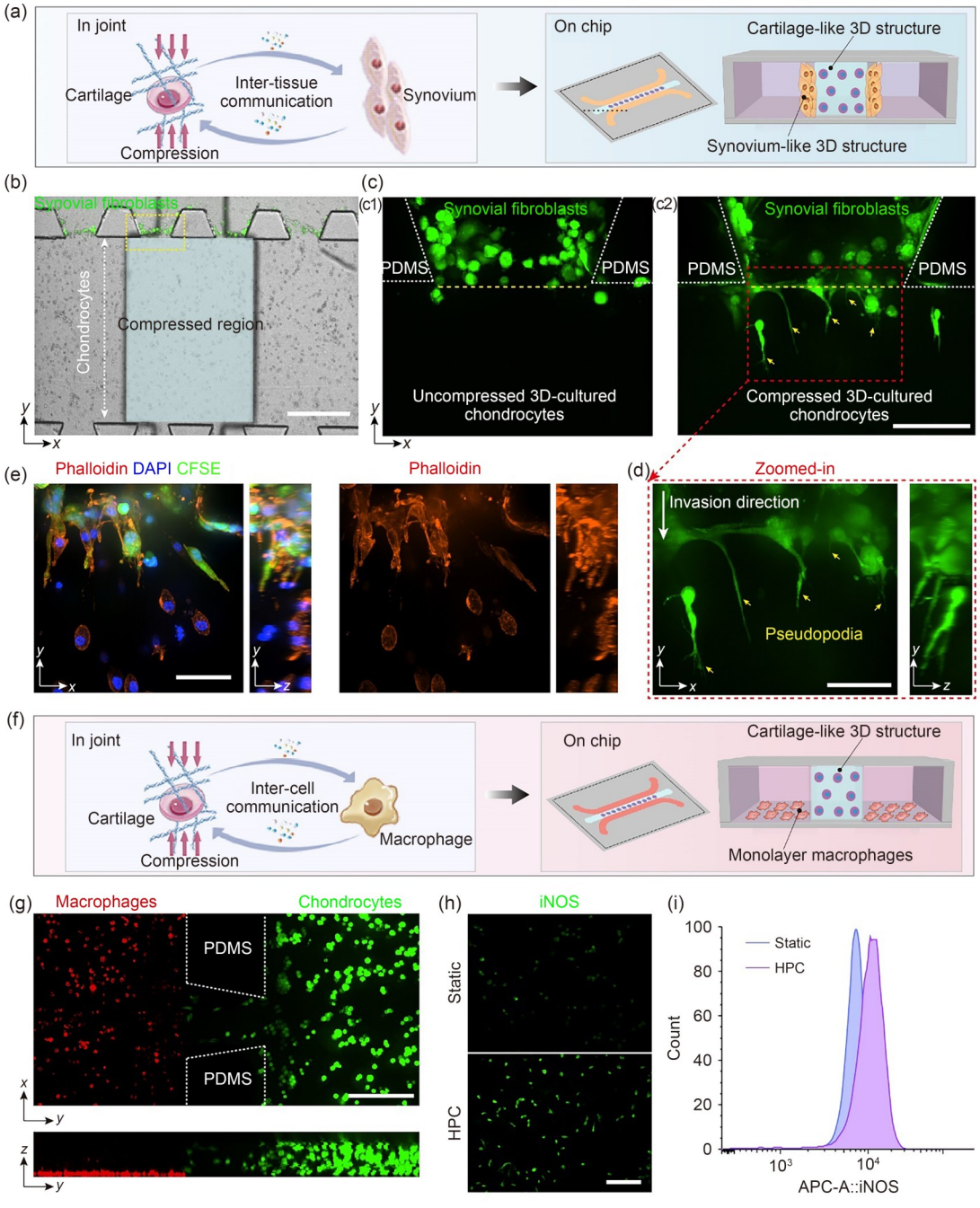

Fig. 5 Establishment of co-culture models integrating mechanical loading and inter-tissue/cell communication function in the chip. (a) Schematic illustrating the construction of a co-culture model of cartilage and synovium in the chip. (b) Confocal image showing the compartmentalized co-culture of chondrocytes and synovial fibroblasts (green) in the chip. The pale blue box indicates the mechanically compressed region. Scale bar: 500 μm. (c) Representative confocal maximum-intensity projection showing the morphology of synovial fibroblasts (green) co-cultured with uncompressed (c1) and compressed (c2) chondrocytes at 17 h post-seeding. White dashed lines outline the boundaries of the PDMS micropillars. Yellow dotted lines indicate the hydrogel boundary (n=7–8). Scale bar: 100 μm. (d) Magnified confocal image corresponding to the red-dotted box region in panel (c). Yellow arrowheads indicate pseudopodial protrusions of synovial fibroblasts invading the hydrogel–chondrocyte composite matrix. Scale bar: 50 μm. (e) Representative confocal immunofluorescence image of F-actin (phalloidin, red) and nuclei (4',6-diamidino-2'-phenylindole (DAPI), blue) showing the actin-rich cell protrusions of CFSE-preloaded synovial fibroblasts (green) co-cultured for 17 h with mechanically overloaded 3D chondrocytes in the chip. Scale bar: 50 μm. (f) Schematic illustrating the construction of a co-culture model of cartilage and macrophages in the chip. (g) Representative confocal maximum-intensity projection of the co-culture of macrophages (red) and chondrocytes (green) within the chip. Scale bar: 200 μm. (h) Representative confocal immunofluorescence images showing iNOS staining in RAW264.7 macrophages (n=3 independent experiments). Top panel: macrophages co-cultured with static (non-overloaded) 3D chondrocytes. Bottom panel: macrophages co-cultured with mechanically loaded 3D chondrocytes. Scale bar: 100 μm. (i) Flow cytometry quantification comparing iNOS expression in RAW264.7 macrophages co-cultured with mechanically overloaded vs. static (non-overloaded) 3D chondrocytes (n=3 independent experiments)

breached the cell–hydrogel matrix interface and penetrated deeply into the matrix (Fig. 5d). Phalloidin staining (Fig. 5e) revealed that the protrusions were actin-rich structures, consistent with the pseudopodia observed in prior studies of fibroblast chemotactic invasion into 3D matrices, where such structures formed at the leading edge to promote directional migration [49–52]. This result suggests that mechanically overloaded chondrocytes induce synovial fibroblasts to extend invasive actin-rich protrusions, forming an invasive front. This finding aligns with the histopathology of synovial tissue in arthritis, which exhibits degradative invasion into adjacent cartilage during progressive joint destruction, as evidenced in in vivo studies [2, 53–56].

Subsequently, we established a separate co-culture model involving cartilage and macrophages (Fig. 5f; Fig. S8 in the supplementary information). Specifically, RAW264.7 macrophages were seeded in both side channels of the cell culture layer after the chondrocytes in the middle channel were subjected to mechanical overload (600 mbar, 0.5 Hz, 4 h per day for 2 d). The spatial distribution of the chondrocytes and macrophages is presented in Fig. 5g and Fig. S9 (supplementary information). After 24 h of co-culture, we examined the effects of mechanical overload-damaged chondrocytes on the macrophages. Immunofluorescence staining and flow cytometry were performed to characterize the expression of inducible nitric oxide synthase (iNOS), a typical marker of the pro-inflammatory phenotype, in RAW264.7 macrophages. We observed markedly increased expression of iNOS in RAW264.7 macrophages co-cultured with mechanical overload-stimulated chondrocytes compared to those co-cultured with uncompressed chondrocytes (Figs. 5h and 5i). These findings demonstrate that mechanical overload induces chondrocytes to promote inflammatory polarization of macrophages, thereby impacting the joint immune microenvironment.

To elucidate the molecular mediators underlying these multicellular interactions, we used a multiplex Luminex assay to assess soluble factor secretion from mechanically overloaded chondrocytes cultured in the chip. This analysis revealed that mechanical overload markedly upregulated chondrocyte secretion of cytokines (tumor necrosis factor-alpha (TNF-α), interleukin-6 (IL-6), interleukin-12 subunit p40 (IL-12p40), and granulocyte colony-stimulating factor (G-CSF)) and chemokines (monocyte chemoattractant protein-1/C-C motif chemokine ligand 2 (MCP-1/CCL2), regulated on activation, normal T-cell expressed and secreted/C-C motif chemokine ligand 5 (RANTES/CCL5), macrophage inflammatory protein-1α/C-C motif chemokine ligand 3 (MIP-1α/CCL3), macrophage inflammatory protein-1β/C-C motif chemokine ligand 4 (MIP-1β/CCL4), and keratinocyte-derived chemokine/C-X-C motif chemokine ligand 1 (KC/CXCL1)) (Fig. S10 in the supplementary information). The upregulated chemokines produced by overloaded 3D-cultured chondrocytes are responsible for inducing the spatial extension of actin-rich pseudopodia by synovial fibroblasts into chondrocyte-laden hydrogels (Figs. 5c–5e), consistent with chemokine gradient-driven chemotaxis. Moreover, the upregulated pro-inflammatory cytokines are associated with macrophage inflammatory polarization (Figs. 5h and 5i), which cooperatively activates certain signaling pathways (e.g., nuclear factor kappa-B (NF-κB) and signal transducer and activator of transcription (STATs)) to induce iNOS expression [1, 57, 58]. This molecular signature provides a compelling explanation for the observed behaviors in both co-culture models: synovial fibroblast invasion and macrophage inflammatory polarization.

We established two co-culture models in the cartilage-on-a-chip platform to investigate the intercellular interactions during pathophysiological processes associated with cartilage injury in OA onset and progression. Direct observation revealed multicellular interactions wherein mechanically overloaded chondrocytes drive synovial fibroblast invasion and polarize macrophages toward a pro-inflammatory phenotype. The concomitant upregulation of pro-inflammatory cytokine and chemokine expressions suggests that injured chondrocytes function as inflammatory signaling hubs, releasing spatially organized cytokine/chemokine ensembles that directly orchestrate these pathological interactions. This establishes a feedforward pathogenic circuit within the chip-mimicked joint microenvironment, recapitulating early OA pathomechanisms where mechano-activated cartilage initiates cross-tissue communication. Compared to conventional co-culture methods such as transwell assays, our models integrate mechanical loading with inter-tissue/cellular communication, key components of the native bio-chemo-mechanical joint microenvironment. Crucially, our chip-based platform enables in situ, real-time monitoring of pathophysiological processes under coupled bio-chemo-mechanical stimuli. This capability provides critical insights into how such integrated stimuli enhance intricate pathogenic mechanisms and profoundly influence OA onset and progression.

2.6 Transcriptional profiling and validation of therapeutic targets in mechanically overloaded chondrocytes

We performed transcriptional analysis of chondrocytes stimulated by mechanical overloading within the chip to detect any changes in molecular signatures underlying cartilage injury in our chip. By analyzing and comparing the transcriptional profiles of chondrocytes in the compressed and uncompressed regions within the chip, we identified 1456 differentially expressed genes (DEGs), including 524 upregulated DEGs and 932 downregulated DEGs (Fig. S11 in the supplementary information). A more detailed Kyoto Encyclopedia of Genes and Genomes (KEGG) pathway analysis

revealed the enrichment of DEGs in biological pathways associated with TNF signaling, cytokine–cytokine receptor interactions, NF-κB signaling, apoptosis, rheumatoid arthritis, and nucleotide oligomerization domain (NOD)-like receptor signaling (Fig. 6a1). In addition, Gene Ontology (GO) analysis highlighted the changes induced by HPC in chondrocytes, which occurred particularly in pathways related to chemokine-mediated signaling and inflammatory responses (Fig. 6a2). The results demonstrated that mechanical overloading triggered the activation of pathways associated with the onset and development of OA in 3D-cultured chondrocytes in the chip. Therefore, the comprehensive transcriptional analysis substantiated that the application of HPC to a 3D cartilage-like microconstruct in our chip may serve to mimic cartilage injury in vivo. Notably, these findings offer a potential explanation for the aforementioned phenomena in the biomimetic co-culture model, including the invasive behavior of synovial fibroblasts and the inflammatory polarization of macrophages. As demonstrated in previous studies, the activation of these pathways in chondrocytes may result in the production of secreted substances by these cells, which could act as endogenous danger signals to stimulate the activity of other cells in the joint [2, 58, 59].

By performing gene set enrichment analysis (GSEA), we identified the activation of two pathways, the canonical Wnt pathway and the NF-κB pathway, in chondrocytes stimulated by HPC (Fig. 6b). As previous studies have indicated, both pathways can be excessively activated by mechanical overloading, leading to cartilage injury that is detrimental to joint health and associated with OA [60]. Specifically, the Wnt pathway, an important pathway in cartilage development and homeostasis, can also be excessively activated by mechanical overloading [6, 60]. Similarly, the NF-κB pathway, a well-known inflammatory pathway, can be activated by excessive mechanical loading, leading to cartilage destruction, the expression of pro-inflammatory genes, and inhibition of ECM synthesis, thus promoting the progression of OA [35, 61, 62]. The immunofluorescence results revealed increased accumulation of β-catenin in the nucleus, indicating enhanced activation of the canonical Wnt signaling pathway upon mechanical overload (Fig. 6c; Fig. S12 in the supplementary information). In addition, enhanced activation of the NF-κB pathway under mechanical overloading was evidenced by increased nuclear accumulation of NF-κB.

In addition to physiological studies of OA using our multifunctional cartilage-on-a-chip, it could be utilized for testing potential drug candidates for OA treatment. To demonstrate this capability, we investigated the preventive effects of adavivint (a canonical Wnt pathway inhibitor) and sulfasalazine (an NF-κB pathway inhibitor) against cartilage injury induced by mechanical overload. In OA pathogenesis, mechanical overload leads to chondrocyte dysfunction and inflammation through intricate networks of downstream signaling pathways [6]. Regulating the rebalance of these pathways is currently one of the main strategies for treating OA. Based on the confirmation of the activation of both of these pathways in chondrocytes subjected to mechanical overload in our chips, we evaluated the effectiveness of adavivint and sulfasalazine to prevent cartilage injury by rebalancing cartilage homeostasis between the anabolism and catabolism of chondrocytes. We used immunofluorescence to assess the production of collagen II, aggrecan, and MMP-13, which are commonly used to represent the anabolism and catabolism of chondrocytes. The results revealed that both drugs upregulated collagen II and aggrecan production while downregulating MMP-13 expression (Figs. 6d and 6e), indicating a protective effect on chondrocytes against mechanical overload. These findings are consistent with those of previous preclinical and clinical studies that have demonstrated the chondroprotective effects of these drugs in OA treatment [63–65]. Therefore, the validation substantiated that our chip can serve as an effective pharmacological testing platform for OA therapeutic candidates.

Using the microfluidic chip, we successfully developed a multifunctional in vitro microphysiological system. This cartilage-on-a-chip enables precise control of the mechanical compression applied to 3D-cultured cells using compressed air, a common approach in microfluidic devices that provide mechanical stimuli, and allows real-time, in situ monitoring of mechanotransduction responses at the single-cell level [8, 22, 26, 28]. The multichannel design allows for the co-culture of different cell types, such as cartilage with synovium or macrophages, enabling the in vivo-like study of intercellular interactions. This integration provides the potential for investigating the detailed pathogenesis of disease onset and development, as well as for evaluating potential drug candidates for OA, in a close-to-in vivo microenvironment.

Based on the aforementioned functional validations, our chip exhibits several potential applications in disease mechanism research and therapeutic strategy development. First, our cartilage-on-a-chip platform can simulate a microenvironment encountered by cartilage in vivo and therefore facilitates in-depth studies on the occurrence and progression of OA within a bio-chemo-mechanical microenvironment. In particular, the integration of mechanical cues may considerably aid the discovery of new pathogenic mechanisms and contribute to the development of novel therapeutic drugs [66]. Furthermore, the controlled mechanical loading applied to individual 3D-cultured cells in the chip enables the regulation of cellular responses through varying levels of mechanical stimulation. For example, physiological doses of mechanical stimulation can help halt disease progression and promote cartilage tissue regeneration by enhancing chondrocyte anabolism. This provides guidance for OA patients to engage in appropriate exercise regimens [5]. In addition, treatment strategies targeting reduced tissue strain, such as weight loss,

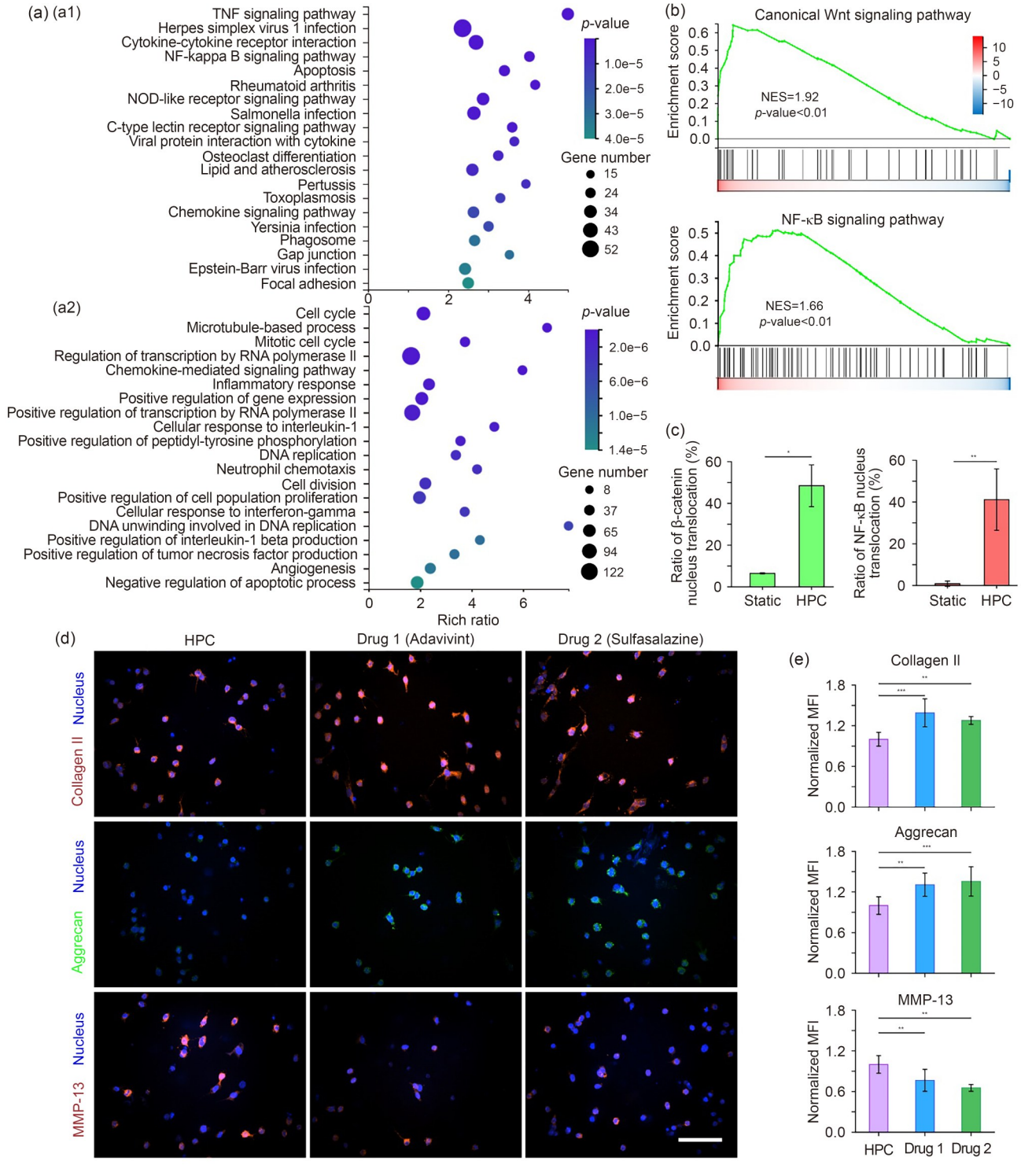

Fig. 6 Transcriptional analysis and validation of potential candidates for OA treatment using the multifunctional cartilage-on-a-chip. (a) KEGG (a1) and GO (a2) enrichment analyses of DEGs from transcriptional analysis of chondrocytes stimulated by HPC (600 mbar, 0.5 Hz, 4 h per day) on the chip. $p \leqslant 0.05$ and absolute $\log_2$(fold change)$\geqslant 1$. (b) Gene set enrichment analysis (GSEA) plot of the KEGG/GO pathways in chondrocytes stimulated by HPC compared to unstimulated chondrocytes. Genes showed marked enrichment in the canonical Wnt signaling pathway (top) and NF-κB signaling pathway (bottom). (c) Quantification of the ratio of nuclear to cytoplasmic β-catenin (left) and NF-κB (right) in chondrocytes under HPC and static conditions. Data represent the mean±standard error of the mean (SEM) (n=3 independent experiments). Statistical significance was determined by Student's t-test. $^{*}p<0.05$ and $^{**}p<0.01$. (d) Immunofluorescence of collagen II, aggrecan, and MMP-13 in chondrocytes under different drug treatments. Scale bar: 100 μm. (e) Quantification of collagen II, aggrecan, and MMP-13 expression levels in chondrocytes based on the fluorescence intensity in (d). Data represent the mean±SEM (n=3 independent experiments). Statistical significance was determined by one-way analysis of variance (ANOVA), followed by Tukey's post hoc test for pairwise comparisons. $^{**}p<0.01$ and $^{***}p<0.001$. NES: normalized enrichment score

can be implemented for patients with OA induced by obesity, thereby mitigating aberrant downstream signaling induced by mechanical overload [6]. Moreover, the functionality of our chip for real-time, in situ studies of single-cell behavior aids in the elucidation of how individual cells perceive and respond to external stimuli, including ECM and mechanical compression. This feature paves the way for the development of 3D cell culture biomaterials such as hydrogels. Finally, our multifunctional chip, which integrates tissue microenvironment mimicry and single-cellular response studies, opens new avenues for investigating other diseases and evaluating drug candidates, such as skin and cardiovascular diseases.

As with any model, the current version of our multifunctional microfluidic chip and the analysis presented in this work had several limitations, particularly compared with the complexity of articular cartilage in vivo. First, the clinical relevance of the in vitro model established in our microfluidic chip could be enhanced by replacing mouse chondrocytes with those derived from patient cartilage tissues. Furthermore, the simple UV-curable GelMA hydrogel used in this study could be upgraded to a hydrogel that incorporates articular cartilage-specific ECM components. Second, other kinds of mechanical stimulation, such as shear force, could be incorporated into the chip to recapitulate the complex mechanical conditions in vivo. Furthermore, while our multifunctional chip provides basic co-culture capability, a critical feature for studying OA-related crosstalk, a more sophisticated co-culture set-up consisting of macrophages, endothelial cells, and fibroblasts could be designed to better simulate the complex microenvironment found in joints. Finally, the multifunctional microfluidic chip could be modified to a higher-throughput version by integrating multiple actuation compartments in one chip to achieve a miniaturized in vitro model.

3 Conclusions

In summary, we have developed an integrated cartilage-on-a-chip that functions as an in vitro model to emulate the microphysiological bio-chemo-mechanical signals during the pathogenesis of OA. By using this chip, we established a cartilage injury model by precisely controlling the magnitude and spatial localization of mechanical compression. Importantly, the unique advantages of this model system enable the visualization of dynamic cellular responses, especially mechanotransduction and inter-tissue or intercellular communication, following mechanical stimulation at a systemic level, thereby overcoming some of the limitations of in vivo animal models and the currently available in vitro models. These advancements will facilitate further insights into the pathophysiology of OA, particularly its onset, and aid in the development of new therapeutics. Furthermore, the approach presented in this work is immediately applicable to a wide range of other diseases by modeling the microphysiological processes involved in bio-chemo-mechanical-coupled microenvironments.

4 Experimental section

4.1 Microfluidic chip design and fabrication

The master molds for the pressurization actuation compartment layer and the cell culture layer were fabricated using standard photolithography techniques with an SU-8 2150 photoresist (Microchem, USA) on 100-mm silicon wafer substrates. The cell culture layer features three parallel channels separated by two rows of trapezoidal PDMS columns. The middle channel has the dimensions of approximately 1.5 mm in width and approximately 0.1 mm in height, and the side channels have a width of approximately 2.5 mm and a height of approximately 0.1 mm. The channel in the pressurization actuation compartment layer was approximately 0.1 mm high. The overlapping area between the middle channel at the bottom and the pressurization actuation compartment at the top consisted of three rectangles, each measuring approximately 1.0 mm in width and approximately 1.5 mm in length (Fig. S13 in the supplementary information). The surfaces of the silicon masters were rendered hydrophobic using trichloro (1H, 1H, 2H, 2H-perfluorooctyl) silane (Sigma-Aldrich, Germany) at 120 °C for 5 min. After cooling to room temperature, the master molds were used to prepare the PDMS components of the chip.

The PDMS components were fabricated using the same polymerization scheme. Specifically, the PDMS (184 silicone elastomer; Dow Corning, USA) base was thoroughly mixed with a curing agent at a mass ratio of 10:1. To achieve a cell culture layer with controllable thickness, the bubble-free PDMS mixture was poured onto the master and then spun at 100 r/min for 60 s followed by 300 r/min for 60 s. For the pressurization actuation compartment, the master was placed in a dish, and the bubble-free PDMS mixture was poured onto it. Subsequently, the master coated with PDMS mixture was polymerized by thermal curing at 65 °C for 3 h on a hot plate. The PDMS slab with the desired microfluidic features was then peeled from the silicon master.

The sandwich-like chip was assembled layer by layer. First, the PDMS slab of the pressurization actuation compartment was manually punched using a 0.7-mm-diameter puncher and bound to the closed surface of the PDMS slab of the cell culture layer. The bound layers were then punched to create inlet and outlet holes corresponding to the three channels in the cell culture layer using a 1.2-mm-diameter puncher. Next, the bottom surface of the perforated double-layer structure was bound to a standard glass microscope

slide (approximately 0.13–0.17 mm). Finally, the top surface of the sandwich-like structure was bound to two rectangular PDMS slabs containing three through circular holes, each with a diameter of 3.5 mm. These holes served as media reservoirs during chip culture to supply enough fluid, such as the cell culture medium. All bonding steps were performed using plasma treatment for 1 min. Post-fabrication, the fully assembled chip was strengthened at 80 °C for 2 h.

Before being used for cell experiments, the microfluidic chip was subjected to sterilization. The specific procedure involved injecting 75% disinfection alcohol into the channels of the cell culture layer using a pipette and allowing it to stand at room temperature for 2 h. Subsequently, the phosphate-buffered saline (PBS) solution was injected into the channels of the cell culture layer using a pipette and allowed to stand at room temperature for 1 h. Subsequently, the liquid in the chip was dried on a hot plate at a temperature of 65 °C. It was then placed on a cell operation table for UV irradiation for at least 1 h before being used for the cell culture experiments.

4.2 Cell isolation and culture

Primary mouse chondrocytes were harvested from the articular cartilage of mice aged 3–5 d old [67], as approved by the Biological and Medical Ethics Committee of Beihang University (BM20200107). The isolated primary chondrocytes were then seeded in a 10-cm dish and cultured in Dulbecco's modified Eagle medium/nutrient mixture F-12 (DMEM/F12) containing 10% (volume fraction) fetal bovine serum (FBS) (Gibco, USA) and 1% (volume fraction) penicillin/streptomycin (Solarbio, China). Primary mouse fibroblast-like synoviocytes were purchased from Procell Life Science and Technology Co., Ltd., China, and were expanded in complete medium. The murine macrophage cell line RAW264.7 (RRID: CVCL_0493) was purchased from Yuchi Biotechnology Co., Ltd., China, and cultured in DMEM supplemented with 10% FBS and 1% penicillin/streptomycin. Mycoplasma contamination was routinely monitored using a Mycoplasma Stain Assay Kit (Beyotime Biotechnology, China). For the passaging experiments, cells were enzymatically detached from the dish by treating them with trypsin-ethylenediaminetetraacetic acid (EDTA) solution for 1 min at 37 °C. After centrifugation, the cell pellet was resuspended in the culture medium. All cells were maintained at 37 °C in an incubator under a 5% CO_2 atmosphere.

4.3 On-chip cell culture

To construct the hydrogel-based 3D cartilage-like microconstruct on the microfluidic chip, we employed a UV-curable GelMA hydrogel following the manufacturer's instructions (EFL, China). In brief, the GelMA solution was prepared by weighing the required mass of GelMA into a centrifugal tube, adding a 2.5 mg/mL standard solution of initiator lithium phenyl-2, 4, 6-trimethylbenzoylphosphinate (LAP) into the tube, and thoroughly mixing to ensure complete infiltration of the GelMA. The tube was then heated and dissolved in a 65 °C water bath for 25 min, shielded from light, with intermittent shaking. The GelMA solution was immediately sterilized using a 0.22 μm sterile needle filter.

Primary mouse chondrocytes were suspended in GelMA solution (0.1 g/mL) pre-warmed at 37 °C to achieve a cell density of approximately 4×10^6 cells/mL. This cell suspension was then injected into the middle channel of the cell culture layer. Subsequently, UV irradiation at 405-nm light was applied for 10 s at a power of 3 W, leading to hydrogel polymerization and the formation of a stable and uniform hydrogel-based 3D cartilage-like microconstruct, aided by PDMS trapezoidal pillars. The medium was injected into the two side channels, and the chip was placed in a 37 °C incubator for 5 min before washing and removal of the medium. To ensure adequate nutrient supply for chondrocytes, four 100 μL pipette tips filled with the medium were vertically inserted at the entrance of the two side channels of the cell culture layer. The chip was then placed in a cell incubator (37 °C, 5% CO_2), and the medium was changed every other day to maintain cell viability while minimizing the contamination risks associated with external perfusion pumps, thus simplifying the operational process.

To construct the co-culture model of cartilage–synovium within the multifunctional chip, primary mouse chondrocytes (approximately 4×10^6 cells/mL) were initially seeded into the middle channel to form the hydrogel-based 3D cartilage-like microconstruct, as described above. Primary mouse synovial fibroblasts were then resuspended in a cell culture medium at a density of approximately 2×10^6 cells/mL, and the mixture was injected into the two side channels. After injection, the chip was manually rotated 90° and treated by orbital shaking for 10 min at 100 r/min to trap the fibroblasts in the groove among the PDMS trapezoidal pillars of the chip and to allow them to attach to the surface of the erect side walls of the 3D hydrogel scaffold. The chips were then kept in cell culture incubators at 5% CO_2 and 37 °C.

Similarly, to construct the co-culture model of cartilage-macrophages, the mouse macrophage cell line RAW264.7 was integrated into the multifunctional chip following the establishment of the hydrogel-based 3D cartilage-like microconstruct, as described above. Specifically, the macrophages were resuspended in the cell culture medium at a density of approximately 4×10^6 cells/mL, and the mixture was injected into the two side channels pre-coated with fibronectin (50 μg/mL). After macrophage attachment, two pipette tips containing 200 μL of the culture medium were inserted vertically into the inlet of the chip, and the chip was placed in an incubator at 5% CO_2 and 37 °C.

4.4 Application and characterization of mechanical compression loading

Mechanical compression was induced in the chip's pressurization chamber through compressed air supplied by an electro-pneumatic pressure flow controller (OB1 MK3+, Elveflow, France). The complete system configuration is illustrated in Fig. S14 (supplementary information). 3D images of the hydrogel within the middle channel of the cell culture layer before and after compression were obtained using a microscope (Ti2 Eclipse, Nikon, Japan) with a 20× air objective (numerical aperture (NA) =0.5) and a spinning disk confocal system. Fluorescent polystyrene nanoparticles with a diameter of 100 nm (Thermo Fisher Scientific, USA) were incorporated into the hydrogel solution before injection into the chip channels. We used a 488-nm laser to image the hydrogel with fluorescent tracer particles at a 1-μm *z*-axis interval.

The deformation of the hydrogel under mechanical compression was then quantified by analyzing the 3D images. NIS-Elements software was used to directly determine the thickness of the hydrogel, and we quantified the compressive deformation of the hydrogel by comparing the variation in the thickness of the hydrogel under the deformed and initial states. In addition, we quantified the spatial distribution of the compressive strain by tracking individual fluorescent particles embedded in the hydrogel [68–70]. The displacements of those particles were used to calculate the local strain using a Lagrange finite strain tensor [68].

We also obtained 3D images of cells embedded in the hydrogel using the confocal microscope. In detail, the fluorescent red dye 1,1'-dioctadecyl-3,3,3',3'-tetramethylindodicarbocyanine,4-chlorobenzenesulfonate salt (DiD; Beyotime Biotechnology) was used to label the primary mouse chondrocyte membranes. The stained cells were then mixed with 10% GelMA hydrogel, and the cell-hydrogel mixture was slowly injected into the middle channels of the chip and photocrosslinked under UV light at a power of 3 W for 10 s. The culture medium was injected into both side channels of the cell culture layer. 3D images of cells were then obtained with a 40× air objective (NA=0.75) at a 0.4-μm *z*-axis interval. The deformation of 3D cells embedded in the hydrogel under mechanical compression was quantified by comparing the variations in cell thickness (i.e., the dimension of the cells along the direction of hydrogel compression) under the deformed and initial states.

4.5 Cell viability assay

Live/Dead staining was performed to evaluate the cell viability of GelMA-encapsulated chondrocytes cultured in the chip for different durations. The assay was performed using a calcein-acetoxymethyl ester/propidium iodide (Calcein-AM/PI) Live/Dead Cell Staining Kit (Solarbio), where live cells were stained green with Calcein-AM and dead cells were stained red with PI. In brief, the culture medium in the chip was removed using a pipette, and PBS was injected for two washes, with each wash incubated at 37 °C for 15 min. The prepared Calcein-AM staining working solution was then added to both side channels, followed by a 2-h incubation at 37 °C in dark conditions. Subsequently, the Calcein-AM staining working solution was aspirated, and a diluted PI staining working solution was added and then incubated at room temperature in dark conditions for 10 min. After incubation, the staining working solution was removed, and the cells were washed twice with PBS, with each wash being incubated at 37 °C for 15 min. Laser confocal microscopy was then employed for imaging.

For quantitative assessment of cell proliferation and long-term survival, cell counting was conducted based on confocal imaging of Hoechst-stained nuclei, with staining performed separately at 0, 7, and 21 d post-seeding. In brief, at each time point, the culture medium was removed from the chip, and samples were washed twice with PBS (37 °C, 15 min each). A Hoechst 33342 working solution (Solarbio) was then added to the channels, and the samples were incubated at 37 °C in dark conditions for 30 min. Excess dye was aspirated, followed by two additional PBS washes (37 °C, 15 min each). Confocal imaging for cell counting was performed using a 20× air objective (NA=0.75), with 3D Z-stacks acquired at 0.9 μm/step over a fixed 110 μm depth. Each imaging field was standardized to 900 pixel×700 pixel (1 pixel= 0.55 μm) to ensure a consistent spatial range, capturing all cells within the defined 3D field (lateral: 900 pixel×700 pixel; axial: 110 μm).

4.6 On-chip immunofluorescent staining and analysis

Upon completion of the cell culture experiments, the culture medium within the channels of the chip was removed, and PBS was slowly injected into both side channels for washing. Cells were fixed in 4% paraformaldehyde at room temperature for 60 min, followed by serial washes with PBS. For intracellular targets, cells were permeabilized with 0.2% Triton X-100 PBS solution for 30 min. Subsequently, to block nonspecific binding, cells were incubated with 10% goat serum blocking buffer at room temperature for 2 h. Subsequently, the corresponding primary antibodies were added and incubated overnight at 4 °C. The following primary antibodies were used: fluorescein isothiocyanate (FITC)-labeled phalloidin (Solarbio), donor and tetramethylrhodamine-5-(and 6-) isothiocyanate (TRITC)-labeled phalloidin (Solarbio), rabbit anti-mouse collagen II (Proteintech, China), rabbit anti-mouse aggrecan (Proteintech), rabbit anti-mouse

MMP-13 (Proteintech), rabbit anti-mouse ADAMTS5 (Abcam, USA), rabbit anti-mouse Piezo1 (Proteintech), rabbit anti-mouse iNOS (Proteintech), rabbit anti-mouse β-catenin (Cell Signaling, USA), and rabbit anti-mouse NF-κB p65 (Cell Signaling). Following serial washes with PBS, the appropriate secondary antibodies labeled with DyLight 488 and DyLight 550 (BOSTER, China) were added to the chip and incubated at room temperature for 2 h in the dark. Cell nuclei were stained with DAPI (Solarbio) at room temperature for 10 min, followed by serial washes with PBS. The samples were kept in the dark until imaging was performed.

For imaging acquisition, immunofluorescence images were acquired using a Nikon Ti2 Eclipse microscope equipped with a 20× air objective (NA=0.75). Confocal Z-stacks were captured with a step size of 0.9 μm. Each chip contained three mechanical loading regions, and one cross-sectional image (spanning the full thickness of the hydrogel) was acquired from each region to ensure representative sampling of the hydrogel and encapsulated cells.

For image processing, visualization (e.g., Z-stack rendering) was conducted using NIS-Elements software (Version AR 5.21.03 64-bit, Nikon). To generate 2D composite images for subsequent quantification, confocal 3D stacks were first processed using the "Create HDR from Current ND" function in the software's "Applications" module, followed by maximum-intensity projection to compress the 3D stack into a single 2D maximum-intensity projection image.

Quantitative analysis was performed using Fiji ImageJ software (National Institutes of Health, USA). Prior to quantification, background subtraction was implemented by selecting cell- and hydrogel-free blank areas to define background fluorescence, which was subsequently subtracted from the entire image. Fluorescent signal intensities were then quantified using the "Measure" tool in Fiji ImageJ, with the signal thresholds maintained consistently across all samples. Each group included at least three independent biological replicates, and three technical replicates were analyzed per biological replicate.

4.7 Calcium imaging and analysis

For intracellular calcium imaging, chondrocytes embedded in the hydrogel within the middle channel of the chip were loaded with Calbryte^{TM} 520 AM (AAT Bioquest, USA) after Day 1 of culture and underwent serial washes with fresh Hanks' balanced salt solution with HEPES (HHBS) buffer. Specifically, the Calbryte^{TM} 520 AM working solution (5 μmol/L) was injected into both side channels of the chip. Subsequently, the dye-loaded chips were incubated at 37 °C for 90 min and washed three times with fresh HHBS buffer to eliminate any residual calcium dye. To record the changes in fluorescence intensity within the cells under mechanical compression, live-cell imaging was performed using a confocal microscope (Nikon) to capture Z-stacks of cells at 10-min intervals over time. The intracellular concentration of calcium was assessed by quantifying the fluorescence intensity in the cells using Fiji ImageJ software [71, 72].

4.8 Soluble factor Luminex multiplex assay

Primary mouse chondrocytes (approximately 4×10^6 cells/mL) were seeded into the middle channel to establish hydrogel-based 3D-cultured chondrocytes. Mechanical overload (600 mbar, 0.5 Hz, 4 h per day) was applied to the chondrocyte-laden hydrogels for 2 d. Following mechanical stimulation, the fluid in both side channels was replaced with fresh culture medium. After 24 h of incubation, the culture medium was harvested and centrifuged at 4 °C. The supernatant was collected and stored at −80 °C until Luminex analysis, which was conducted by LabEx (Shanghai, China). A Bio-Plex Pro Mouse Cytokine 23-plex kit (Bio-Rad, #M60009RDPD) was used to measure the concentrations of cytokines and chemokines in the supernatant according to the manufacturer's protocol. The analyte panel included TNF-α, interferon (IFN)-γ, G-CSF, granulocyte-macrophage colony-stimulating factor (GM-CSF), IL-1α, IL-1β, IL-2, IL-3, IL-4, IL-5, IL-6, IL-9, IL-10, IL-12p40, IL-12p70, IL-13, CCL2 (MCP-1), CCL3 (MIP-1α), CCL4 (MIP-1β), CCL5 (RANTES), CCL11 (eotaxin), and CXCL1 (KC). Data acquisition was performed using a Luminex-200 system (Luminex Corporation, USA), with subsequent analysis using Milliplex Analyst v5.1 software (MilliporeSigma, USA).

4.9 Flow cytometry analysis

Macrophages were harvested from both side channels in the chips by trypsin digestion. After serial washes with PBS, the cells were blocked with anti-CD16/CD32 (Fcγ III/II receptor) (BD Biosciences, USA) for 15 min at room temperature. Subsequently, 250 μL of fixation/permeabilization solution (BD Biosciences) was added to the cells. After incubation at 4 °C for 20 min, the cells were washed with 1× BD Perm/Wash^{TM} buffer and incubated with phycoerythrin (PE)-conjugated anti-mouse iNOS (eBioscience, USA) for 30 min at room temperature. The cells were then washed with 1× BD Perm/Wash^{TM} buffer and measured using a FACS Canto II flow cytometer (BD Biosciences). Finally, the data were analyzed using FlowJo software (BD Biosciences).

4.10 Transcriptomic and gene expression analyses

After applying mechanical compression (600 mbar, 0.5 Hz for 4 h), the chondrocyte–hydrogel block was obtained from the compressed and uncompressed areas within a chip by

peeling off the sandwich structure. The chondrocytes were released and collected from the block using GelMA lysis buffer at 37 °C for 3 min. These cells were shipped on ice to Beijing Easyresearch Technology Limited, China, for the Smart-seq2 experiments [73]. In brief, single cells were sorted into an ice-cold cell lysis buffer containing Triton X-100, oligo-dT primers, deoxy-ribonucleoside triphosphates (dNTPs), and ribonuclease (RNase) inhibitor. All subsequent steps were performed on ice to preserve RNA integrity. Reverse transcription was initiated by adding a reaction mixture comprising Superscript II reverse transcriptase, RNase inhibitor, DTT, betaine, $MgCl_2$, TSO, and Superscript II first-strand buffer. The reaction was performed at 25 °C for 5 min, followed by 42 °C for 60 min, 50 °C for 30 min, and finally 72 °C for 10 min. Polymerase chain reaction (PCR) preamplification was carried out using KAPA HiFi HotStart ReadyMix (KAPA Biosystems, South Africa) for 22 cycles, where the IS PCR primer concentration was reduced to 50 nmol/L. The cycling conditions included four cycles at 98 °C for 20 s, 65 °C for 30 s, and 72 °C for 5 min, followed by 18 cycles of 98 °C for 20 s, 67 °C for 15 s, and 72 °C for 5 min, with a final extension step at 72 °C for 5 min. Subsequently, the amplified samples were purified twice using AMPure XP beads (Beckman Coulter, USA). The quality of amplified products was assessed using FragmentAnalyzer 1.0.2.9, and the fragments were mostly larger than 1 kb. For library construction, cDNA fragmentation was achieved by incubation at 55 °C for 10 min. PCR enrichment was performed under the following conditions: hot lid at 105 °C; initial denaturation at 72 °C for 3 min; enzyme activation at 98 °C for 30 s; then 5–15 cycles consisting of 98 °C for 15 s, 60 °C for 30 s, and 72 °C for 3 min, with a final extension step at 72 °C for 5 min, and holding at 4 °C. The amplified products were purified and size-selected using AMPure XP magnetic beads. Library quality control and quantification were conducted as follows: the fragment size distribution was analyzed using FragmentAnalyzer 1.0.2.9, which confirmed that the majority of fragments ranged between 300 and 700 bp in size. Quantitative analysis was performed using Qubit fluorometry. Sequencing was carried out on the NovaSeq platform with paired-end 150-bp reads (PE150). The gene expressions were compared between the chondrocytes in the compressed and uncompressed areas within the chip using DESeq2.

4.11 Drug treatment

Two compounds, adavivint (MedChemExpress, USA) and sulfasalazine (MedChemExpress), were evaluated in a cartilage injury model induced by mechanical overload within the chip. In detail, primary mouse chondrocytes were seeded in the middle channel of the chip for 14 d, after which the medium was supplemented with each compound separately (adavivint, 100 nmol/L; sulfasalazine, 100 μmol/L) for 7 d while applying the HPC regimen (600 mbar, 0.5 Hz, 4 h per day), with the medium replaced every 48 h. After drug treatment, chondrocytes were fixed for cell immunofluorescence analysis to assess the preventive effects of the agents on chondrocyte injury induced by HPC by characterizing the expression of collagen II, aggrecan, and MMP-13.

4.12 Statistical analyses

All statistical analyses were performed using Origin 2018 software, and the results were presented as mean±standard error of the mean (SEM). Statistical significance of differences was assessed using Student's *t*-test or one-way analysis of variance (ANOVA). Different significance levels (*p*-values) were indicated in each figure using asterisks ($^{*}p<0.05$, $^{**}p<0.01$, and $^{***}p<0.001$).

Supplementary Information The online version contains supplementary material available at https://doi.org/10.1631/bdm.2500348.

Acknowledgements This work was supported by the National Natural Science Foundation of China (Nos. 12072010 and 11674019), the Fundamental Research Funds for the Central Universities (No. YWF-22-K-101), and the National Key Research and Development Program of China (No. 2022YFB3804300). We acknowledge the helpful conversations with Prof. Lingqian Chang and Dr. Yuqiong Wang from Beihang University, and with Prof. Ting Cao and Dr. Chen Yang from Institute of Physics, Chinese Academy of Sciences.

Author contributions Conceptualization: HXJ, TJW, and YX. Methodology: HXJ, TJW, and YX. Formal analysis: HXJ, LMD, TJW, and YX. Investigation: HXJ, SHY, HG, KQS, FRK, and TT. Supervision: TJW and YX. Writing—original draft: HXJ and YX. Writing—review and editing: QTZ, TJW, and YX.

Declarations

Conflict of interest The authors declare that they have no conflict of interest.

Ethical approval The animal experiments for the isolation of primary mouse chondrocytes were carried out with the approval of the Biological and Medical Ethics Committee at Beihang University (approval No. BM20200107).

Data availability The data that support the findings of this study are available from the corresponding authors upon reasonable request.

Use of generative AI tools During the preparation of this work, the authors used ChatGPT and Grammarly in order to improve language and check for grammatical errors. After using these tools, the authors reviewed and edited the content as needed and take full responsibility for the content of the publication.

References

1. Paggi CA, Teixeira LM, Le Gac S et al (2022) Joint-on-chip platforms: entering a new era of in vitro models for arthritis. *Nat Rev Rheumatol* 18(4):217–231. https://doi.org/10.1038/s41584-021-00736-6

2. Sanchez-Lopez E, Coras R, Torres A et al (2022) Synovial inflammation in osteoarthritis progression. *Nat Rev Rheumatol* 18(5):258–275. https://doi.org/10.1038/s41584-022-00749-9
3. Delco ML, Bonassar LJ (2021) Targeting calcium-related mechanotransduction in early OA. *Nat Rev Rheumatol* 17(8):445–446. https://doi.org/10.1038/s41584-021-00649-4
4. Wang N, Lu YF, Rothrauff BB et al (2023) Mechanotransduction pathways in articular chondrocytes and the emerging role of estrogen receptor-α. *Bone Res* 11(1):13. https://doi.org/10.1038/s41413-023-00248-x
5. Goldring SR, Goldring MB (2016) Changes in the osteochondral unit during osteoarthritis: structure, function and cartilage-bone crosstalk. *Nat Rev Rheumatol* 12(11):632–644. https://doi.org/10.1038/nrrheum.2016.148
6. Latourte A, Kloppenburg M, Richette P (2020) Emerging pharmaceutical therapies for osteoarthritis. *Nat Rev Rheumatol* 16(12): 673–688. https://doi.org/10.1038/s41584-020-00518-6
7. Xie RJ, Yao H, Mao AS et al (2021) Biomimetic cartilage-lubricating polymers regenerate cartilage in rats with early osteoarthritis. *Nat Biomed Eng* 5(10):1189–1201. https://doi.org/10.1038/s41551-021-00785-y
8. Occhetta P, Mainardi A, Votta E et al (2019) Hyperphysiological compression of articular cartilage induces an osteoarthritic phenotype in a cartilage-on-a-chip model. *Nat Biomed Eng* 3(7): 545–557. https://doi.org/10.1038/s41551-019-0406-3
9. Maleiner B, Tomasch J, Heher P et al (2018) The importance of biophysical and biochemical stimuli in dynamic skeletal muscle models. *Front Physiol* 9:1130. https://doi.org/10.3389/fphys.2018.01130
10. Griffin TM, Guilak F (2005) The role of mechanical loading in the onset and progression of osteoarthritis. *Exerc Sport Sci Rev* 33(4):195–200. https://doi.org/10.1097/00003677-200510000-00008
11. Banh L, Cheung KK, Chan MWY et al (2022) Advances in organ-on-a-chip systems for modelling joint tissue and osteoarthritic diseases. *Osteoarthr Cartil* 30(8):1050–1061. https://doi.org/10.1016/j.joca.2022.03.012
12. Petta D, D'Amora U, D'Arrigo D et al (2022) Musculoskeletal tissues-on-a-chip: role of natural polymers in reproducing tissue-specific microenvironments. *Biofabrication* 14(4):042001. https://doi.org/10.1088/1758-5090/ac8767
13. Zheng FY, Fu FF, Cheng Y et al (2016) Organ-on-a-chip systems: microengineering to biomimic living systems. *Small* 12(17): 2253–2282. https://doi.org/10.1002/smll.201503208
14. Wu QR, Liu JF, Wang XH et al (2020) Organ-on-a-chip: recent breakthroughs and future prospects. *Biomed Eng Online* 19(1):9. https://doi.org/10.1186/s12938-020-0752-0
15. Bhatia SN, Ingber DE (2014) Microfluidic organs-on-chips. *Nat Biotechnol* 32(8):760–772. https://doi.org/10.1038/nbt.2989
16. Ma C, Peng YS, Li HT et al (2021) Organ-on-a-chip: a new paradigm for drug development. *Trends Pharmacol Sci* 42(2):119–133. https://doi.org/10.1016/j.tips.2020.11.009
17. Jalili-Firoozinezhad S, Miranda CC, Cabral JMS (2021) Modeling the human body on microfluidic chips. *Trends Biotechnol* 39(8): 838–852. https://doi.org/10.1016/j.tibtech.2021.01.004
18. Huh D, Matthews BD, Mammoto A et al (2010) Reconstituting organ-level lung functions on a chip. *Science* 328(5986):1662–1668. https://doi.org/10.1126/science.1188302
19. Cao T, Shao CM, Yu XY et al (2022) Biomimetic alveolus-on-a-chip for SARS-CoV-2 infection recapitulation. *Research* 2022: 9819154. https://doi.org/10.34133/2022/9819154
20. Amartumur S, Nguyen H, Huynh T et al (2024) Neuropathogenesis-on-chips for neurodegenerative diseases. *Nat Commun* 15(1):2219. https://doi.org/10.1038/s41467-024-46554-8
21. Hu Y, Zhang H, Wang SC et al (2023) Bone/Cartilage organoid on-chip: construction strategy and application. *Bioact Mater* 25: 29–41. https://doi.org/10.1016/j.bioactmat.2023.01.016
22. Paggi CA, Hendriks J, Karperien M et al (2022) Emulating the chondrocyte microenvironment using multi-directional mechanical stimulation in a cartilage-on-chip. *Lab Chip* 22(9): 1815–1828. https://doi.org/10.1039/d1lc01069g
23. Rothbauer M, Byrne RA, Schobesberger S et al (2021) Establishment of a human three-dimensional chip-based chondro-synovial coculture joint model for reciprocal cross talk studies in arthritis research. *Lab Chip* 21(21):4128–4143. https://doi.org/10.1039/d1lc00130b
24. Mondadori C, Palombella S, Salehi S et al (2021) Recapitulating monocyte extravasation to the synovium in an organotypic microfluidic model of the articular joint. *Biofabrication* 13(4):045001. https://doi.org/10.1088/1758-5090/ac0c5e
25. Rothbauer M, Höll G, Eilenberger C et al (2020) Monitoring tissue-level remodelling during inflammatory arthritis using a three-dimensional synovium-on-a-chip with non-invasive light scattering biosensing. *Lab Chip* 20(8):1461–1471. https://doi.org/10.1039/c9lc01097a
26. Paggi CA, Venzac B, Karperien M et al (2020) Monolithic microfluidic platform for exerting gradients of compression on cell-laden hydrogels, and application to a model of the articular cartilage. *Sens Actuat B Chem* 315:127917. https://doi.org/10.1016/j.snb.2020.127917
27. Rosser J, Bachmann B, Jordan C et al (2019) Microfluidic nutrient gradient–based three-dimensional chondrocyte culture-on-a-chip as an in vitro equine arthritis model. *Mater Today Bio* 4:100023. https://doi.org/10.1016/j.mtbio.2019.100023
28. Lee D, Erickson A, You T et al (2018) Pneumatic microfluidic cell compression device for high-throughput study of chondrocyte mechanobiology. *Lab Chip* 18(14):2077–2086. https://doi.org/10.1039/c8lc00320c
29. Petta D, D'Arrigo D, Salehi S et al (2024) A personalized osteoarthritic joint-on-a-chip as a screening platform for biological treatments. *Mater Today Bio* 26:101072. https://doi.org/10.1016/j.mtbio.2024.101072
30. Onal S, Alkaisi MM, Nock V (2022) Microdevice-based mechanical compression on living cells. *iScience* 25(12):105518. https://doi.org/10.1016/j.isci.2022.105518
31. Mainardi A, Börsch A, Occhetta P et al (2025) An organ-on-chip platform for strain-controlled, tissue-specific compression of cartilage and mineralized osteochondral interface to study mechanical overloading in osteoarthritis. *Adv Healthc Mater* 14(23): 2501588. https://doi.org/10.1002/adhm.202501588
32. Zhen GH, Guo QY, Li YS et al (2021) Mechanical stress determines the configuration of TGFβ activation in articular cartilage. *Nat Commun* 12(1):1706. https://doi.org/10.1038/s41467-021-21948-0

33. Thompson CL, Chapple JP, Knight MM (2014) Primary cilia disassembly down-regulates mechanosensitive hedgehog signalling: a feedback mechanism controlling ADAMTS-5 expression in chondrocytes. *Osteoarthr Cartil* 22(3):490–498. https://doi.org/10.1016/j.joca.2013.12.016
34. Clarke J (2021) Bone stresses out cartilage in OA. *Nat Rev Rheumatol* 17(5):250. https://doi.org/10.1038/s41584-021-00612-3
35. Hodgkinson T, Kelly DC, Curtin CM et al (2022) Mechanosignalling in cartilage: an emerging target for the treatment of osteoarthritis. *Nat Rev Rheumatol* 18(2):67–84. https://doi.org/10.1038/s41584-021-00724-w
36. Wieland HA, Michaelis M, Kirschbaum BJ et al (2005) Osteoarthritis—an untreatable disease? *Nat Rev Drug Discov* 4(4):331–344. https://doi.org/10.1038/nrd1693
37. Shi YY, Hu XQ, Cheng J et al (2019) A small molecule promotes cartilage extracellular matrix generation and inhibits osteoarthritis development. *Nat Commun* 10(1):1914. https://doi.org/10.1038/s41467-019-09839-x
38. Lee W, Leddy HA, Chen Y et al (2014) Synergy between Piezo1 and Piezo2 channels confers high-strain mechanosensitivity to articular cartilage. *Proc Natl Acad Sci USA* 111(47):E5114–E5122. https://doi.org/10.1073/pnas.1414298111
39. Savadipour A, Nims RJ, Rashidi N et al (2023) Membrane stretch as the mechanism of activation of PIEZO1 ion channels in chondrocytes. *Proc Natl Acad Sci USA* 120(30):e2221958120. https://doi.org/10.1073/pnas.2221958120
40. Lee W, Nims RJ, Savadipour A et al (2021) Inflammatory signaling sensitizes Piezo1 mechanotransduction in articular chondrocytes as a pathogenic feed-forward mechanism in osteoarthritis. *Proc Natl Acad Sci USA* 118(13):e2001611118. https://doi.org/10.1073/pnas.2001611118
41. Cartes-Saavedra B, Ghosh A, Hajnóczky G (2025) The roles of mitochondria in global and local intracellular calcium signalling. *Nat Rev Mol Cell Biol* 26(6):456–475. https://doi.org/10.1038/s41580-024-00820-1
42. Chen YS, Yu YK, Wen Y et al (2022) A high-resolution route map reveals distinct stages of chondrocyte dedifferentiation for cartilage regeneration. *Bone Res* 10(1):38. https://doi.org/10.1038/s41413-022-00209-w
43. Li H, Jiang XF, Xiao YB et al (2023) Combining single-cell RNA sequencing and population-based studies reveals hand osteoarthritis-associated chondrocyte subpopulations and pathways. *Bone Res* 11(1):58. https://doi.org/10.1038/s41413-023-00292-7
44. Jiang YZ, Tuan RS (2015) Origin and function of cartilage stem/progenitor cells in osteoarthritis. *Nat Rev Rheumatol* 11(4):206–212. https://doi.org/10.1038/nrrheum.2014.200
45. Gan YB, He J, Zhu J et al (2021) Spatially defined single-cell transcriptional profiling characterizes diverse chondrocyte subtypes and nucleus pulposus progenitors in human intervertebral discs. *Bone Res* 9(1):37. https://doi.org/10.1038/s41413-021-00163-z
46. Baker BM, Chen CS (2012) Deconstructing the third dimension: how 3D culture microenvironments alter cellular cues. *J Cell Sci* 125(Pt 13):3015–3024. https://doi.org/10.1242/jcs.079509
47. Roelofs AJ, Zupan J, Riemen AHK et al (2017) Joint morphogenetic cells in the adult mammalian synovium. *Nat Commun* 8:15040. https://doi.org/10.1038/ncomms15040
48. Piluso S, Li Y, Abinzano F et al (2019) Mimicking the articular joint with in vitro models. *Trends Biotechnol* 37(10):1063–1077. https://doi.org/10.1016/j.tibtech.2019.03.003
49. Linder S, Cervero P, Eddy R et al (2023) Mechanisms and roles of podosomes and invadopodia. *Nat Rev Mol Cell Biol* 24(2):86–106. https://doi.org/10.1038/s41580-022-00530-6
50. Lauzier A, Charbonneau M, Harper K et al (2011) Formation of invadopodia-like structures by synovial cells promotes cartilage breakdown in collagen-induced arthritis: involvement of the protein tyrosine kinase Src. *Arthritis Rheum* 63(6):1591–1602. https://doi.org/10.1002/art.30305
51. Sibony-Benyamini H, Gil-Henn H (2012) Invadopodia: the leading force. *Eur J Cell Biol* 91(11–12):896–901. https://doi.org/10.1016/j.ejcb.2012.04.001
52. Caswell PT, Zech T (2018) Actin-based cell protrusion in a 3D matrix. *Trends Cell Biol* 28(10):823–834. https://doi.org/10.1016/j.tcb.2018.06.003
53. Ospelt C (2017) Synovial fibroblasts in 2017. *RMD Open* 3(2):e000471. https://doi.org/10.1136/rmdopen-2017-000471
54. Buckley CD, Ospelt C, Gay S et al (2021) Location, location, location: how the tissue microenvironment affects inflammation in RA. *Nat Rev Rheumatol* 17(4):195–212. https://doi.org/10.1038/s41584-020-00570-2
55. van der Laan WH, Quax PHA, Seemayer CA et al (2003) Cartilage degradation and invasion by rheumatoid synovial fibroblasts is inhibited by gene transfer of TIMP-1 and TIMP-3. *Gene Ther* 10(3):234–242. https://doi.org/10.1038/sj.gt.3301871
56. Mizoguchi F, Slowikowski K, Wei K et al (2018) Functionally distinct disease-associated fibroblast subsets in rheumatoid arthritis. *Nat Commun* 9(1):789. https://doi.org/10.1038/s41467-018-02892-y
57. Wang S, Lu MK, Wang W et al (2022) Macrophage polarization modulated by NF-κB in polylactide membranes-treated peritendinous adhesion. *Small* 18(13):e2104112. https://doi.org/10.1002/smll.202104112
58. Zhang H, Cai D, Bai X (2020) Macrophages regulate the progression of osteoarthritis. *Osteoarthr Cartil* 28(5):555–561. https://doi.org/10.1016/j.joca.2020.01.007
59. Silverstein AM, Stefani RM, Sobczak E et al (2017) Toward understanding the role of cartilage particulates in synovial inflammation. *Osteoarthr Cartil* 25(8):1353–1361. https://doi.org/10.1016/j.joca.2017.03.015
60. Monteagudo S, Lories RJ (2017) Cushioning the cartilage: a canonical Wnt restricting matter. *Nat Rev Rheumatol* 13(11):670–681. https://doi.org/10.1038/nrrheum.2017.171
61. Makarczyk MJ, Hines S, Yagi H et al (2023) Using microphysiological system for the development of treatments for joint inflammation and associated cartilage loss—a pilot study. *Biomolecules* 13(2):384. https://doi.org/10.3390/biom13020384
62. Chang SH, Mori D, Kobayashi H et al (2019) Excessive mechanical loading promotes osteoarthritis through the gremlin-1–NF-κB pathway. *Nat Commun* 10:1442. https://doi.org/10.1038/s41467-019-09491-5
63. Deshmukh V, Hu H, Barroga C et al (2018) A small-molecule inhibitor of the Wnt pathway (SM04690) as a potential disease

modifying agent for the treatment of osteoarthritis of the knee. *Osteoarthr Cartil* 26(1):18–27. https://doi.org/10.1016/j.joca.2017.08.015

64. Deng RH, Zhao RF, Zhang ZN et al (2024) Chondrocyte membrane-coated nanoparticles promote drug retention and halt cartilage damage in rat and canine osteoarthritis. *Sci Transl Med* 16(735):eadh9751. https://doi.org/10.1126/scitranslmed.adh9751
65. Kim SE, Lee JY, Shim KS et al (2018) Attenuation of inflammation and cartilage degradation by sulfasalazine-containing hyaluronic acid on osteoarthritis rat model. *Int J Biol Macromol* 114:341–348. https://doi.org/10.1016/j.ijbiomac.2018.03.059
66. Yang XZ, Chang Y, Wei W (2020) Emerging role of targeting macrophages in rheumatoid arthritis: focus on polarization, metabolism and apoptosis. *Cell Prolif* 53(7):e12854. https://doi.org/10.1111/cpr.12854
67. Gosset M, Berenbaum F, Thirion S et al (2008) Primary culture and phenotyping of murine chondrocytes. *Nat Protoc* 3(8):1253–1260. https://doi.org/10.1038/nprot.2008.95
68. Yang SH, Gerber D, Feng YX et al (2024) Dehydration drives damage in the freezing of brittle hydrogels. *Sci Adv* 10(34): eado7750. https://doi.org/10.1126/sciadv.ado7750
69. Style RW, Boltyanskiy R, German GK et al (2014) Traction force microscopy in physics and biology. *Soft Matter* 10(23):4047–4055. https://doi.org/10.1039/c4sm00264d
70. Kim JY, Heyden S, Gerber D et al (2021) Measuring surface tensions of soft solids with huge contact-angle hysteresis. *Phys Rev X* 11(3):031004. https://doi.org/10.1103/physrevx.11.031004
71. Xie RP, Yu XY, Cao T et al (2023) Fibrous viscoelastic extracellular matrix assists precise neuronal connectivity. *Adv Funct Mater* 33(36):2301926. https://doi.org/10.1002/adfm.202301926
72. Yang C, Wang XC, Xie RP et al (2023) Dynamically reconstructed collagen fibers for transmitting mechanical signals to assist macrophages tracing breast cancer cells. *Adv Funct Mater* 33(9):2211807. https://doi.org/10.1002/adfm.202211807
73. Singh M, Al-Eryani G, Carswell S et al (2019) High-throughput targeted long-read single cell sequencing reveals the clonal and transcriptional landscape of lymphocytes. *Nat Commun* 10(1): 3120. https://doi.org/10.1038/s41467-019-11049-4